SUPPLEMENTARY MATERIAL

Table of Contents

Supplementary Figure Legends

- Figure S1. Illustration of glutaryl-CoA synthetic pathways (related to Figure 1).
- Figure S2. Detection and verification of lysine glutarylation (related to Figure 2).
- Figure S3. SIRT5 catalyzes lysine deglutarylation reactions *in vitro* and *in vivo* (related to Figure 3).
- Figure S4. Enzymology studies on SIRT5-catalyzed deglutarylation (related to Figure4).
- Figure S5. Proteomic and bioinformatic analyses of K_{glu} substrates in SIRT5KO mouse liver (related to Figure 5).
- Figure S6. Carbamoyl Phosphate Synthase 1 is targeted for deglutarylation by SIRT5 (related to Figure 6).
- Figure S7. Physiology and pathophysiology of lysine glutarylation (related to Figure 7).

Supplementary Tables

- Table S1. List of K_{glu} peptides identified by MS from *E. coli* (A) and HeLa cells (B). Annotated MS/MS spectra of the identified Kglu peptides from E. coli (C) and HeLa cells (D) (related to Figure 2).
- Table S2. Enzymology studies on SIRT5-catalyzed deglutarylation (related to Figure4).
- Table S3. List of K_{glu} peptides identified from SIRT5KO mouse liver (related to Figure 5).
- Table S4. Bioinformatic analyses of Kglu substrates (related to Figure 5).
- Table S5. The identifed K_{glu} sites from chemically glutarylated CPS1 (A), glutarylated CPS1 incubated with SIRT5 (B), or glutarylated CPS1 incubated with SIRT3 as a negative control (C) (related to Figure 6).

Supplementary Experimental Procedures

- Reagents
- Chemical and peptide synthesis
- Isotopic labeling using [2, 2, 4, 4-^{2}D] glutarate
- Western blotting analysis, ECL
- Western blotting, LI-COR
- High-pH HPLC fractionation
- In-solution tryptic digestion
- HPLC-MS/MS analysis
- Mass spectrometry data analysis
- Co-elution analysis of K_{glu} peptides by HPLC-MS/MS
- *In vitro* deglutarylation assays
- Principle of fluorescent assay for AMC-based substrates
- Lipofectamin transfection
- Calcium phosphate transfection
- CPS1 immunoprecipitation from mouse liver
- ^{32}P-NAD^{+} consumption assay
- Chemical acylation of BSA and CPS1
- Acylation of histone H4 peptide
- Ammonia measurements
- Ornithine measurements
- CPS1 activity assay
- Protein complex enrichment analysis
- Protein interaction network analysis
- Computational-based molecular modeling
- In silico analysis of deacylation activities of SIRT5
- Fly Stocks and lysate preparation
- Mitochondria isolation from *Drosophila*
- Purification of wild type and inactive mutant hSIRT5 proteins
- Animal experiments
- Functional annotation of K_{glu} proteins
- Enrichment analyses of metabolic pathways using KEGG database
- Domain enrichment analysis using Pfam database
- Protein complexes and interaction networks of lysine glutarylated proteins using CORUM and STRING databases.
- Protein glutarylation

Supplementary References

Supplementary Figure Legends

Figure S1. Illustration of glutaryl-CoA synthetic pathways (related to Figure 1).

Glutaryl-CoA is an intermediate generated from the metabolism of lysine, hydroxylysine and tryptophan.

Figure S2. Detection and verification of lysine glutarylation (related to Figure 2).

(A) Western blot of the whole-cell lysates from bacteria *E. coli,* yeast *S. cerevisiae, Drosophila* S2, mouse MEF, and human HeLa cells. Western blot was performed using the whole-cell lysates from different cells with competition of either tryptic peptides of glutarylated-BSA (right) or tryptic peptides of unmodified-BSA (left).

(B) High resolution MS/MS spectra of a tryptic peptide (NSFTVDIQK$_{+114.0281Da}$NGVK) from the DNA mismatch repair protein Msh2 from HeLa cells with a mass shift of +114.0281 Da at the lysine residue (bottom), the synthetic NSFTVDIQK$_{glu}$NGVK (top). Inset shows the mass-to-charge ratios (m/z) of the precursor ions.

(C) Extracted ion chromatograms (XICs) of the synthetic peptide NSFTVDIQK$_{glu}$NGVK (top), the *in vivo*-derived peptide (middle, from HeLa cells), and their mixture (bottom) by reversed-phase HPLC/MS analysis.

(D) The effects of glutarate on lysine glutarylation. HepG2 cells were treated with 0, 5, and 20 mM glutarate for 24h or 48h, respectively. The global K$_{glu}$ signals showed increases at high glutarate concentrations (20 mM), but not lysine acetylation and lysine succinylation.

(E) Isotopic labeling of K_{glu} peptides. MS/MS spectra of a D_4-glutaryllysine peptide, NFSTVDIQ$K_{D4\text{-}glu}$NGVK from HeLa cells treated with D_4-glutarate.

Figure S3. SIRT5 catalyzes lysine deglutarylation reactions *in vitro* and *in vivo* (related to Figure 3).

(A) HDAC screening schematic. Principle of fluorescent assay for AMC-based substrates were included in the Supplementary Experimental Procedures.

(B) Screening of HDAC *in vitro* lysine deglutarylation activity. Fluorometric assay to detect *in vitro* lysine deglutarylation activities using recombinant HDAC1-11 and SIRT1-7.

(C) ^{32}P-NAD$^+$ consumption monitored by thin layer chromatography after an *in vitro* enzymatic reaction with SIRT3, SIRT4, or SIRT5. We used enzymatically (p300) acylated histone peptide as a substrate; *o*-glutaryl-ADP ribose, OG-ADPR; *o*-succinyl-ADP ribose, OS-ADPR; *o*-acetyl-ADP ribose, OA-ADPR.

(D) HPLC trace of a glutarylated peptide, VKSK_{glu}ATNLWW (HRMS, *m/z*, 637.8480 Da), before and after *in vitro* deglutarylation reaction.

(E) Time course study of SIRT5's lysine deglutarylation activity: the enzymatic reactions were carried out at 37^{o}C for different durations and then deglutarylation products were detected by HPLC/MS.

(F) Dosage of SIRT5 in lysine deglutarylation: enzymatic reactions were carried out with different amount of SIRT5 and then detected by HPLC/MS.

(G) HPLC trace of a glutarylated peptide, VKSK_{glu}ATNLWW (HRMS, m/z, 637.8480 Da, before and after *in vitro* deacylation reactions with HDAC1-11 and SIRT1-7.

Figure S4. Enzymology studies on SIRT5-catalyzed deglutarylation (related to Figure 4).

(A) Lysine side chains derivatized with dicarboxylic acids of varying lengths ranging from 3–6 carbon atoms (i.e., ε-*N*-malonyl-, ε-*N*-succinyl-, ε-*N*-glutaryl-, and ε-*N*-adipoyllysine) were generated. Two series of fluorogenic peptide substrates containing 7-amino-4-methylcoumarin (AMC) were evaluated; one series based on a simple α-*N*-acetylated lysine and one containing the tripeptide sequence, Ac-Leu-Gly-Lys(acyl) (data not shown). Endpoint deacylation assay of mouse or human wild-type SIRT5 or human mutant SIRT5 (HY mutant) against acylated mono-lysine-AMC substrates; K_{ac}, acetyl-lysine; K_{mal}, malonyl-lysine; K_{succ}, succinyl-lysine; K_{glu}, glutaryl-lysine; K_{adi}, adipoyl-lysine. Error bars in this figure and subsequent ones represent standard error of the mean (SEM).

(B) Michaelis-Menten plots for substrates **2**–**4** using human SIRT5 (blue) and murine SIRT5 (red), respectively. The SIRT5 enzyme concentrations were 33 nM (1.0 ng × μL^{-1}) K_{succ} and K_{glu} substrates and 305 nM (9.3 ng × μL^{-1} for the K_{mal} substrate. Fluorescence readings were recorded every 30 seconds for at least 60 min at 25 °C, to obtain initial linear rates **v** (RFU min^{-1}) for each concentration.

(C) Stereoview of the crystal structure of SIRT5 with a glutarylated peptide superimposed in the catalytic pocket.

(D) Comparison of the interactions between SIRT5 and acyl modifications of various lengths. Simplified energy-minimized structures of the interactions between SIRT5 and a histone peptide containing an acetylated, malonylated, succinylated, glutarylated, or

adipoylated Lys residue. Carbon atoms are colored green in SIRT5 residues, magenta in the modified histone peptide residues, or gray in NAD^+. Histone peptide residues are labeled in italics and dashed lines indicated predicted hydrogen bond interactions.
(E) Structural simulation of SIRT5 with acyl lysine residues using AutoDock software (v 4.2). Binding conformations of five acyl lysine residues, lysine acetylation (K_{ac}), butyrylation (K_{bu}), crotonylation (K_{cr}), succinylation (K_{succ}), malonylation (K_{mal}) and glutarylation (K_{glu}), to SIRT5 were analyzed.

Figure S5. Proteomic and bioinformatic analyses of K_{glu} substrates in SIRT5KO mouse liver (related to Figure 5).

(A) Western blotting analysis of mitochondria from *Sirt5*$^{+/+}$ (WT) and *Sirt5*$^{-/-}$ (KO) mouse livers. "WT" and "KO" represent SIRT5 WT and KO mice, respectively. The mitochondria were isolated from WT and SIRT5 KO 48h-fasted mice, and dissolved in SDS sample buffer. Western blotting analysis of mitochondrial protein lysates from WT and SIRT5 KO 48h-fasted mouse livers. The samples were subjected to SDS-PAGE. Western blotting analysis on the samples with anti-K_{succ} antibody.
(B) Western blotting analysis was performed on mitochondrial lysates from mouse brain, heart, gastrocnemius (gastroc) and brown adipose (BAT) tissues in the fed state.
(C) Western blotting analysis was performed on mitochondrial lysates from mouse brain, heart, gastrocnemius (gastroc) and brown adipose (BAT) tissues in the fasted state.
(D) Western blotting analysis of mitochondrial lysates from WT and SIRT5 KO mouse kidneys. Thirty µg of mouse kidney mitochondrial protein lysates were used for the analysis anti-K_{glu}, anti-K_{succ} and anti-K_{ac} antibodies were performed from the

mitochondrial lysates of the same WT or SIRT5 KO mouse Kidney. The Ponceau S loading controls were quantified from the integration of the band image intensity by Bandscan 5.0, showing that the loading of samples are almost equal.

(E) Functional annotation and enrichment analysis of K_{glu} substrates by analyzing gene ontology molecular functions.

(F) Functional annotation and enrichment analysis of K_{glu} substrates by analyzing gene ontology cellular compartments.

(G) Functional annotation and enrichment analysis of K_{glu} substrates by analyzing KEGG metabolic pathways. IPI IDs of Kglu proteins enriched in each pathway are listed in Supplemental Table S4D.

(H) Illustration of enriched KEGG pathways of K_{glu} proteins in valine, leucine and isoleucine degradation. The K_{glu} proteins are indicated by a red star. IPI IDs of the K_{glu} proteins are listed in Supplemental Table S4D.

(I) Illustration of enriched KEGG pathways of K_{glu} proteins in fatty acid metabolism. IPI IDs of the K_{glu} proteins are listed in Supplemental Table S4D.

(J) Illustration of enriched KEGG pathways of K_{glu} proteins in tryptophan metabolism. IPI IDs of the K_{glu} proteins are listed in Supplemental Table S4D.

(K) Illustration of enriched KEGG pathways of K_{glu} proteins in lysine degradation. IPI IDs of the K_{glu} proteins are listed in Supplemental Table S4D.

(L) Enriched domains of K_{glu} proteins from Pfam database.

(M) Enriched protein complexes of K_{glu} proteins from CORUM database.

(N) Interaction network of K_{glu} proteins and their interacting proteins obtained from STRING 9.0 database and visualized in Cytoscape (1,149 of nodes and 5,532 edges). Top 7 most highly ranked clusters are marked in different colors.

(O) Top 7 most highly ranked and tightly connected network clusters from (N) of K_{glu} by MCODE analysis.

Figure S6. Carbamoyl Phosphate Synthase 1 is targeted for deglutarylation by SIRT5 (related to Figure 6).

(A) HeLa cells containing a shScramble (SCR) or shSIRT5 were measured for SIRT5 levels using an anti-SIRT5 antibody.

(B) HEK293 cells containing a shScramble (SCR) or shSIRT5 were measured for protein glutarylation levels using an anti-K_{glu} antibody, protein succinylation using an anti-K_{succ} antibody, and normalized to protein content using an anti-ATP-synthase antibody.

Figure S7. Physiology and pathophysiology of lysine glutarylation (related to Figure 7).

(A) Hepatic whole-cell protein succinylation was measured by immunoblotting with an anti-K_{glu} antibody in two sets (Set1 and Set2) of SIRT5 WT and KO mouse livers that were fed or fasted (48h), respectively. Lysate samples were dissolved in SDS sample buffer and subjected to SDS-PAGE for measurement of protein succinylation using an anti-K_{succ} antibody.

(B) Analysis of liver mitochondrial acyl-CoA levels from mice that were under different fasting conditions. Wide-type mice were fasted for 0h, 6h, 12h, 24h or 48 hours, or the mice were fasted for 24 hours and then re-fed for 3 hours or 6 hours. Total hepatic tissues lysates were analyzed for succinyl-CoA and glutaryl-CoA levels by mass spectrometry metabolomic analysis. Error bars represent SEM.

(C) *Drosophila* were fed with 0X, 1X or 2X tryptophan for 1 week and whole cell lysates were prepared for Western blotting analysis. Samples were analyzed for mitochondrial protein acetylation and succinylation.

(D) CPS1 enzymatic activity was measured in hepatic lysates from wild-type and GCDHKO mice and normalized to total CPS1 protein levels. Error bars represent SEM.

(E) Glutaryl-CoA or glutarate was incubated with heat-inactivated hepatic mitochondrial lysates and measured for total protein by Ponceau S staining.

(F) Glutaryl-CoA, succinyl-CoA, or acetyl-CoA was incubated with BSA and measured for protein glutarylation using an anti-K_{glu} antibody, and normalized to total protein by Ponceau S staining.

Supplementary Tables

Table S1. List of K_{glu} peptides identified by MS from *E. coli* (**A**) and HeLa cells (**B**).

Annotated MS/MS spectra of the identified K_{glu} peptides from *E. coli* **(C)** and HeLa cells **(D)** (related to Figure 2).

Table S2. Enzymology studies on SIRT5-catalyzed deglutarylation. (**A**) Kinetic parameters for SIRT5 deacylation of fluorogenic substrates, based on three individual assays performed in duplicate for K_{succ} and K_{glu}, and two individual assays performed in

duplicate for K_{mal} due to the high amount of enzyme necessary. (**B**) List of k_{cat} and K_M values for SIRT5-catalyzed deacylation (deacetylation, desuccinylation and deglutarylation) with two peptide sequences. For both these two peptides, the catalytic efficiencies for deglutarylation and desuccinylation are comparable, but much higher than that for deacetylation. (**C**) Binding energy of acyl-lysine residues to SIR5 calculated by AutoDock. Compared to K_{ac}, K_{bu}, and K_{cr}, the ligands, K_{mal}, K_{succ}, and K_{glu}, have lower binding energies (related to Figure4).

Table S3. List of K_{glu} peptides identified from SIRT5KO mouse liver (related to Figure 5).

Table S4. Bioinformatic analyses of K_{glu} substrates. **(A)** Enrichment analysis of gene ontology biological processes for K_{glu} proteins. **(B)** Enrichment analysis of gene ontology molecular functions for K_{glu} proteins. **(C)** Enrichment analysis of gene ontology cellular compartment for K_{glu} proteins. **(D)** Enrichment analysis of KEGG pathways for K_{glu} proteins. **(E)** Enrichment analysis of Pfam domains for K_{glu} proteins. **(F)** Enrichment analysis of CORUM core complexes database for K_{glu} proteins. **(G)** Protein network analysis of STRING database by MCODE for K_{glu} proteins (related to Figure 5).

Table S5. The identified K_{glu} sites from chemically glutarylated CPS1 **(A)**, glutarylated CPS1 incubated with SIRT5 **(B)**, or glutarylated CPS1 incubated with SIRT3 as a negative control **(C)** (related to Figure 6).

Supplementary Figure S1

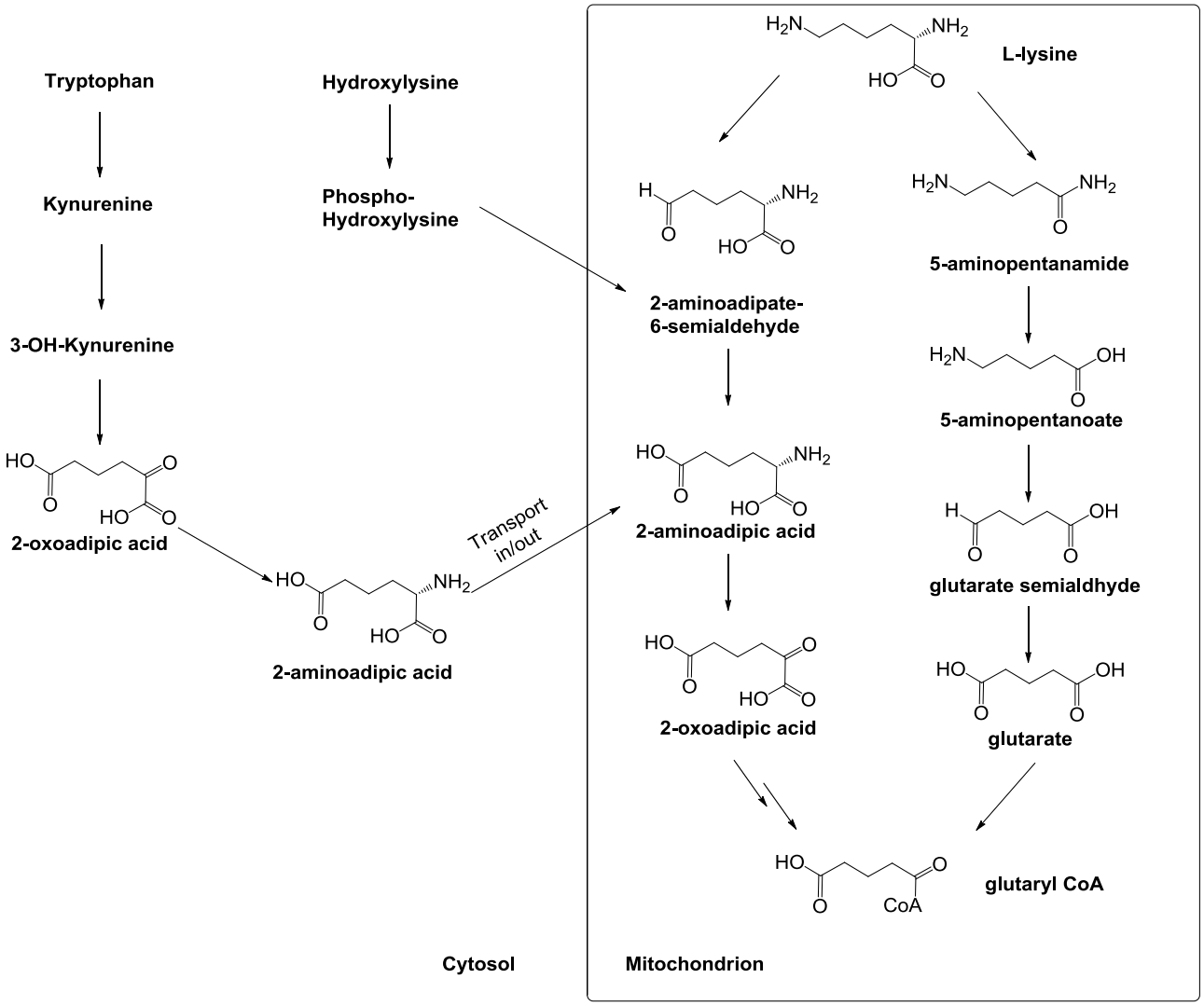

Figure S1 Illustration of glutaryl-CoA synthetic pathways (related to Figure 1). Glutaryl-CoA is an intermediate generated from the metabolism of lysine, hydroxylysine and tryptophan.

Figure S2. Detection and verification of lysine glutarylation (related to Figure 2).

Supplementary Figure S2A

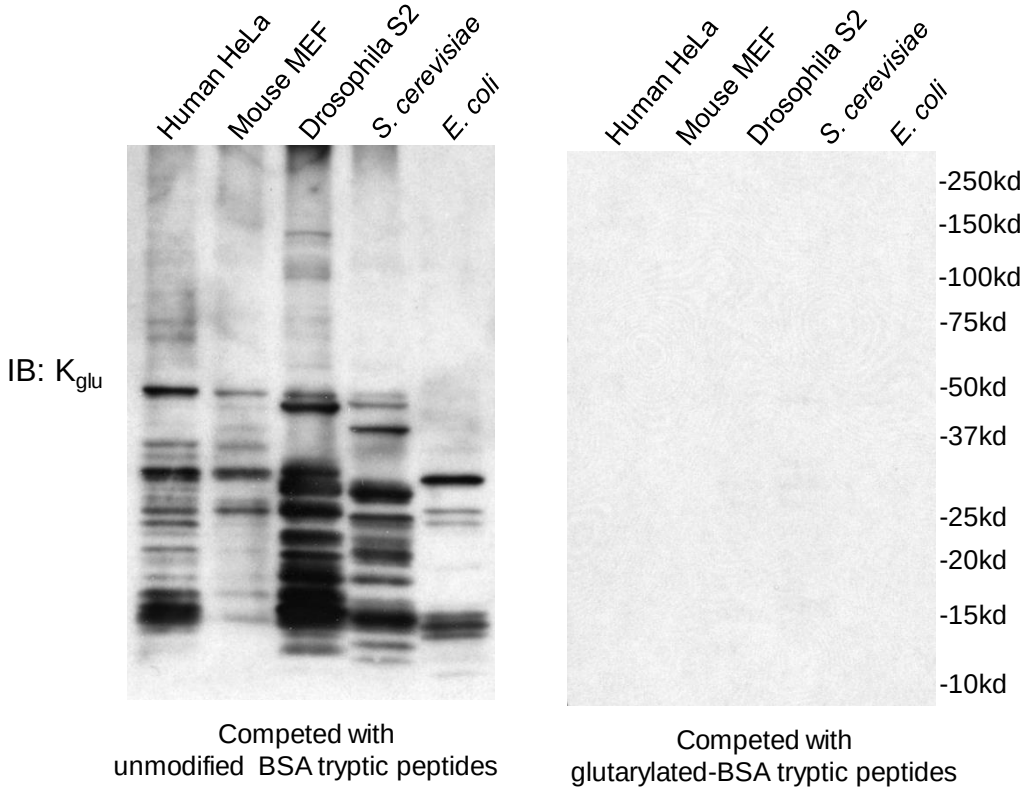

(A) Western blot of the whole-cell lysates from bacteria *E. coli,* yeast *S. cerevisiae, Drosophila* S2, mouse MEF, and human HeLa cells. Western blot was performed using the whole-cell lysates from different cells with competition of either tryptic peptides of glutarylated-BSA (right) or tryptic peptides of unmodified-BSA (left).

Supplementary Figure S2B

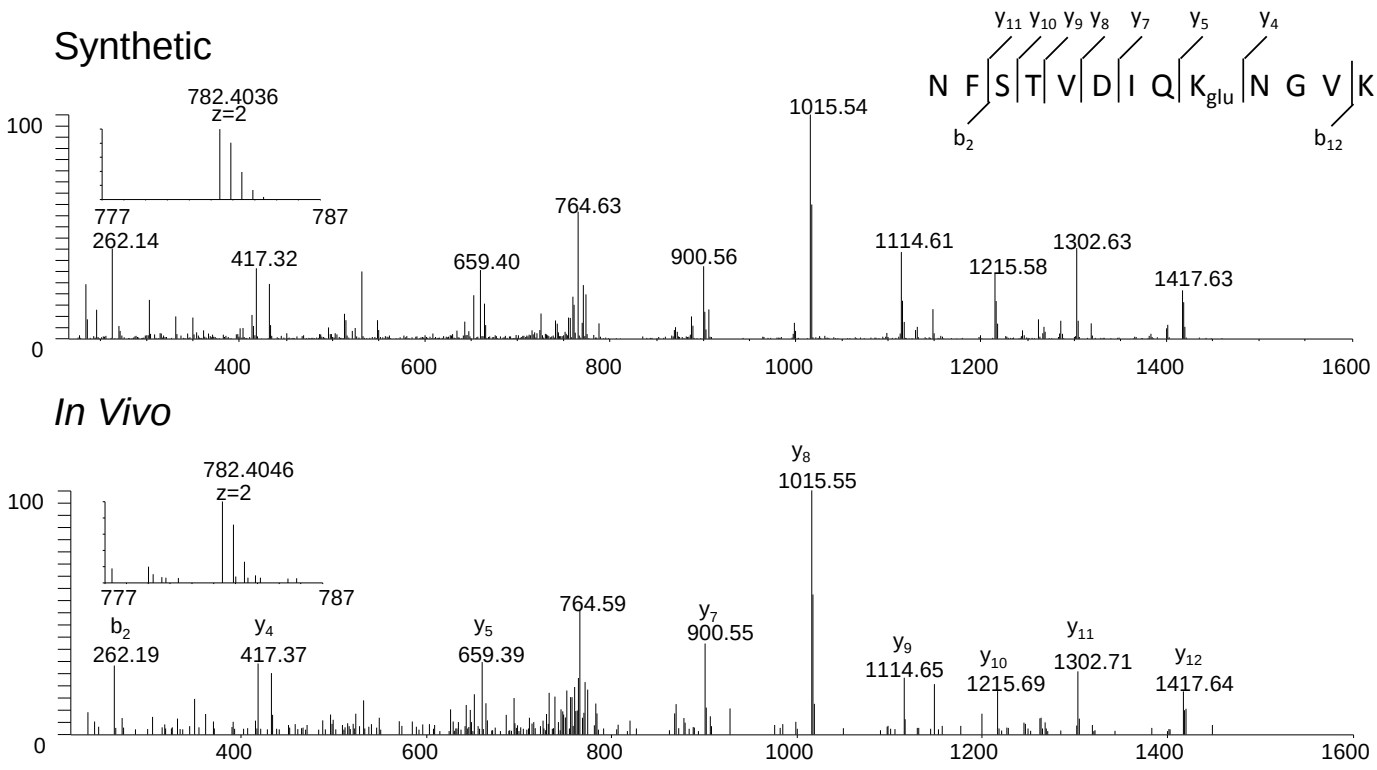

(B) High resolution MS/MS spectra of a tryptic peptide (NSFTVDIQK$_{+114.0281Da}$NGVK) from the DNA mismatch repair protein Msh2 from HeLa cells with a mass shift of +114.0281 Da at the lysine residue (bottom), the synthetic NSFTVDIQK$_{glu}$NGVK (top). Inset shows the mass-to-charge ratios (m/z) of the precursor ions.

Supplementary Figure S2C

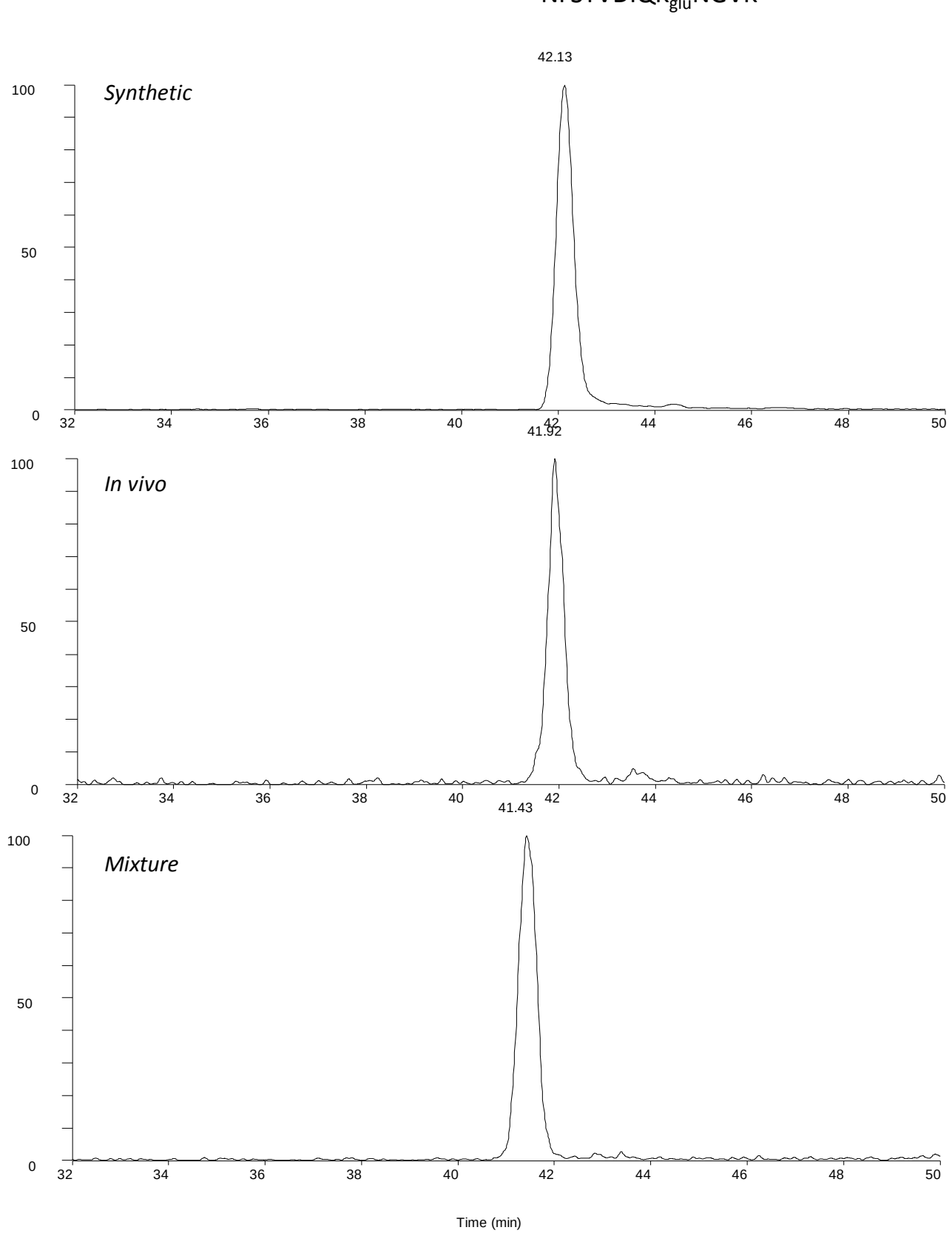

(C) Extracted ion chromatograms (XICs) of the synthetic peptide NSFTVDIQK$_{glu}$NGVK (top), the *in vivo*-derived peptide (middle, from HeLa cells), and their mixture (bottom) by reversed-phase HPLC/MS analysis.

Supplementary Figure S2D

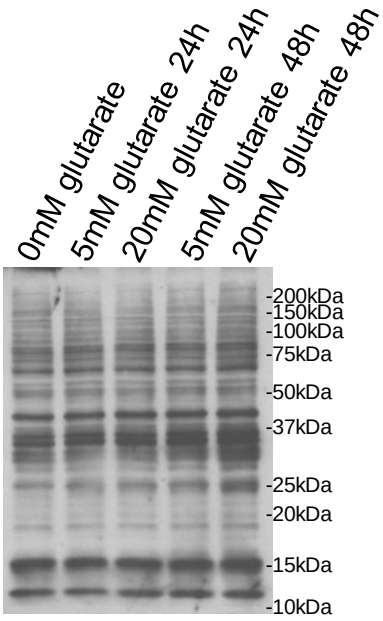

Anti-K_{glu}

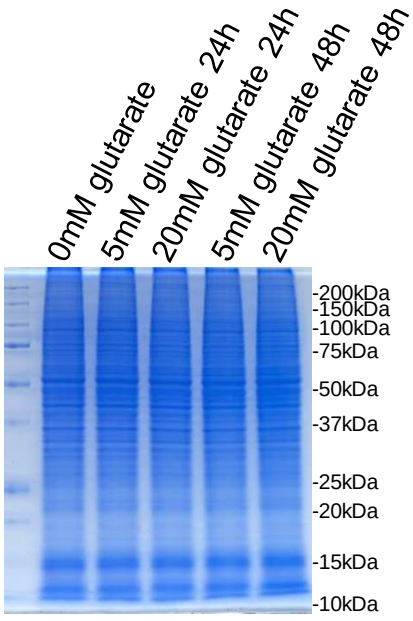

Coomassie Blue

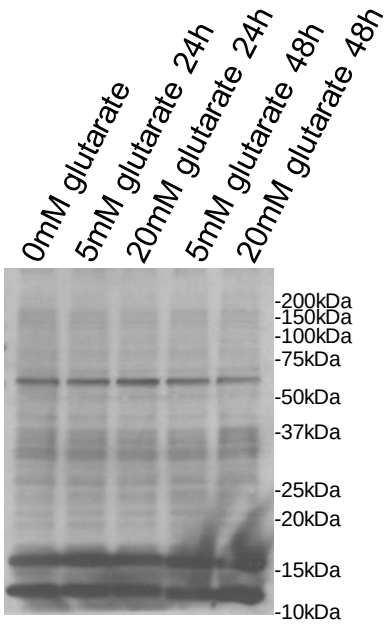

Anti-K_{ac}

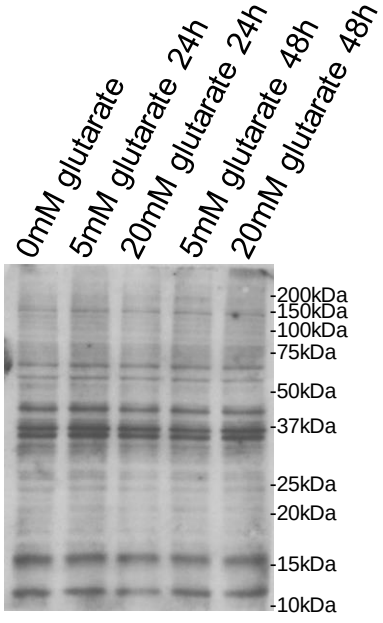

Anti-K_{succ}

(D) The effects of glutarate on lysine glutarylation. HepG2 cells were treated with 0, 5, and 20 mM glutarate for 24h or 48h, respectively. The global K_{glu} signals showed increases at high glutarate concentrations (20 mM), but not lysine acetylation and lysine succinylation.

Supplementary Figure S2E

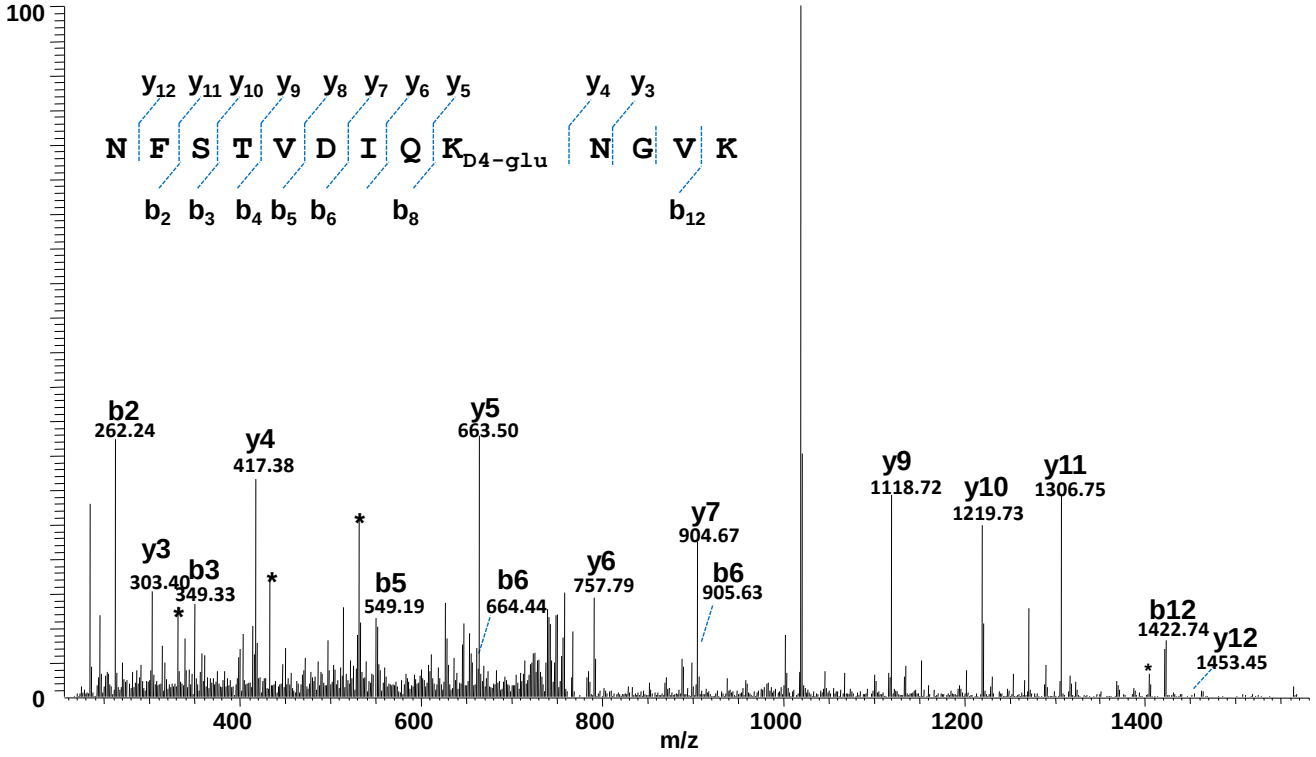

(E) Isotopic labeling of K_{glu} peptides. MS/MS spectra of a D_4-glutaryllysine peptide, NFSTVDIQ$K_{D\text{-}glu}$NGVK from HeLa cells treated with D_4-glutarate.

Figure S3. SIRT5 catalyzes lysine deglutarylation reactions *in vitro* and *in vivo* (related to Figure 3).

Supplementary Figure S3A

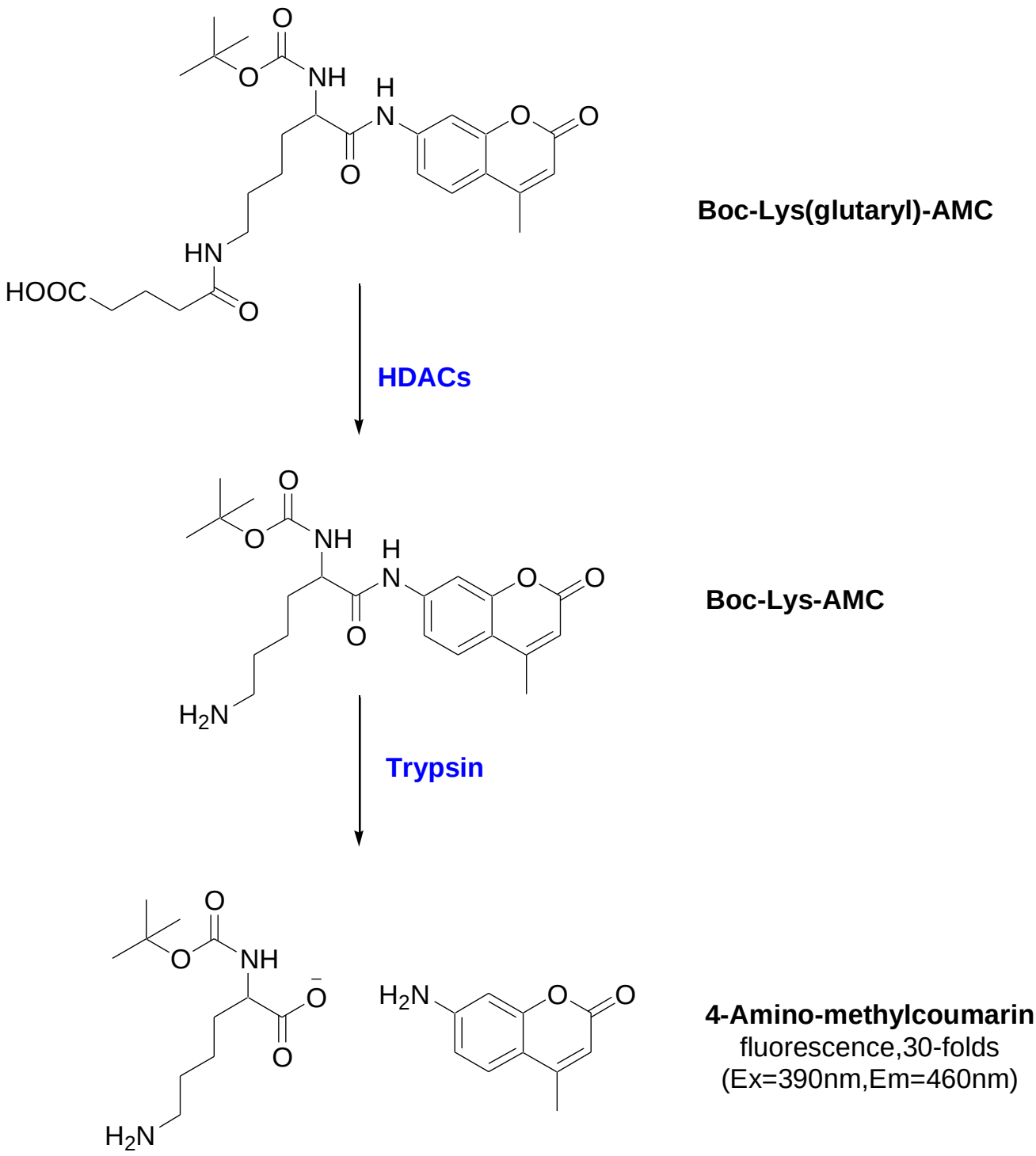

(A) HDAC screening schematic. Principle of fluorescent assay for AMC-based substrates were included in the Supplementary Experimental Procedures.

Supplementary Figure S3B

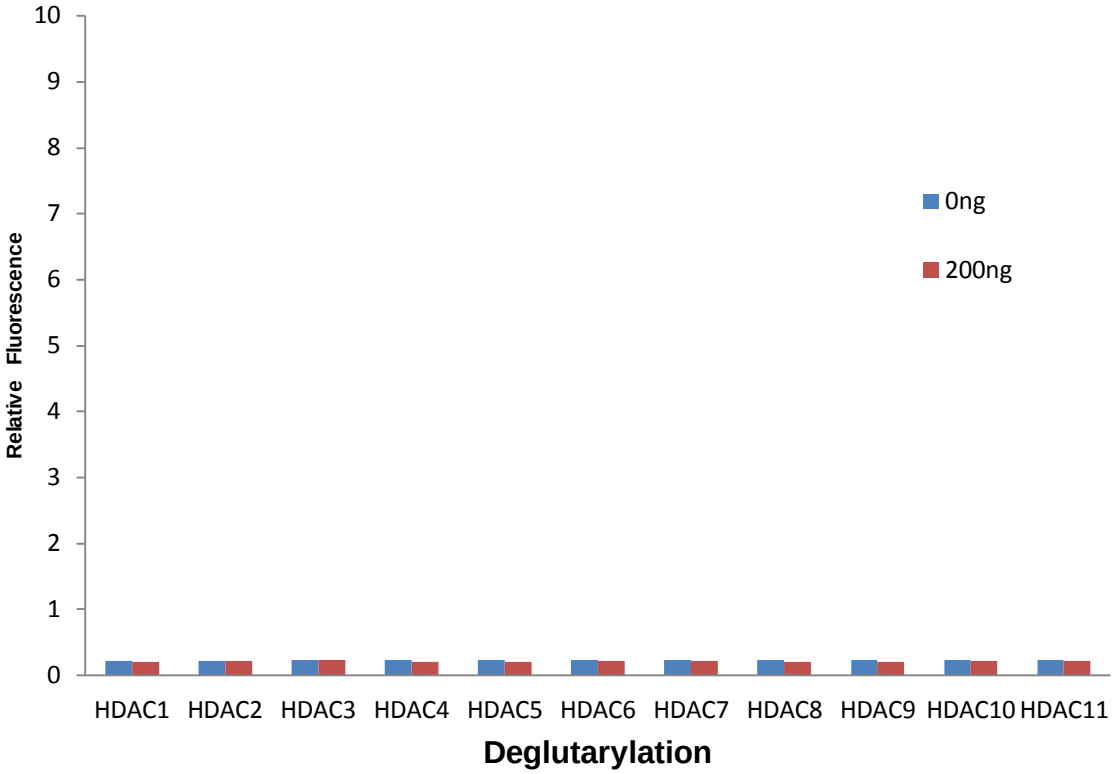

(B) Screening of HDAC lysine deglutarylation activity *in vitro*. Fluorometric assay to detect *in vitro* lysine deglutarylation activities using recombinant HDAC1-11 and SIRT1-7.

Supplementary Figure S3C

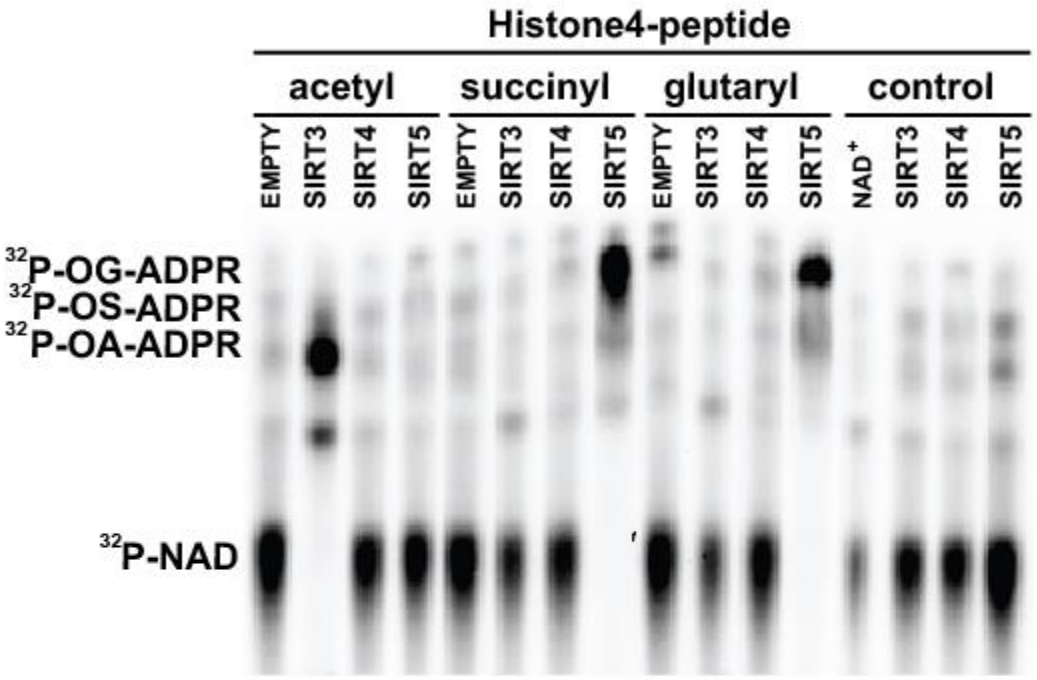

(C) ^{32}P-NAD^{+} consumption monitored by thin layer chromatography after an *in vitro* enzymatic reaction with SIRT3, SIRT4, or SIRT5. We used enzymatically (p300) acylated histone peptide as a substrate; *o*-glutaryl-ADP ribose, OG-ADPR; *o*-succinyl-ADP ribose, OS-ADPR; *o*-acetyl-ADP ribose, OA-ADPR.

Supplementary Figure S3D

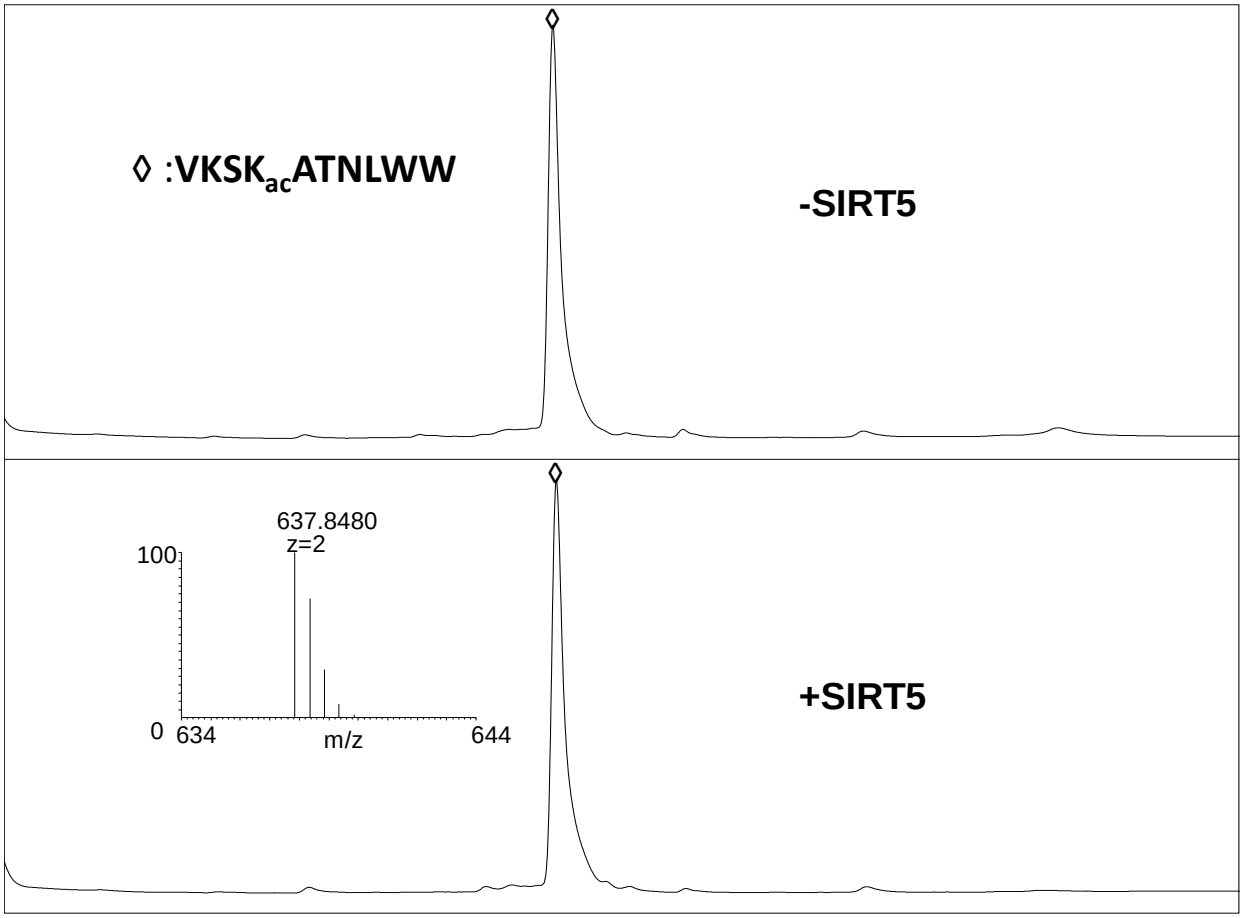

(D) HPLC trace of a glutarylated peptide, VKSK$_{glu}$ATNLWW (HRMS, *m/z*, 637.8480 Da), before and after *in vitro* deglutarylation reaction.

Supplementary Figure S3E

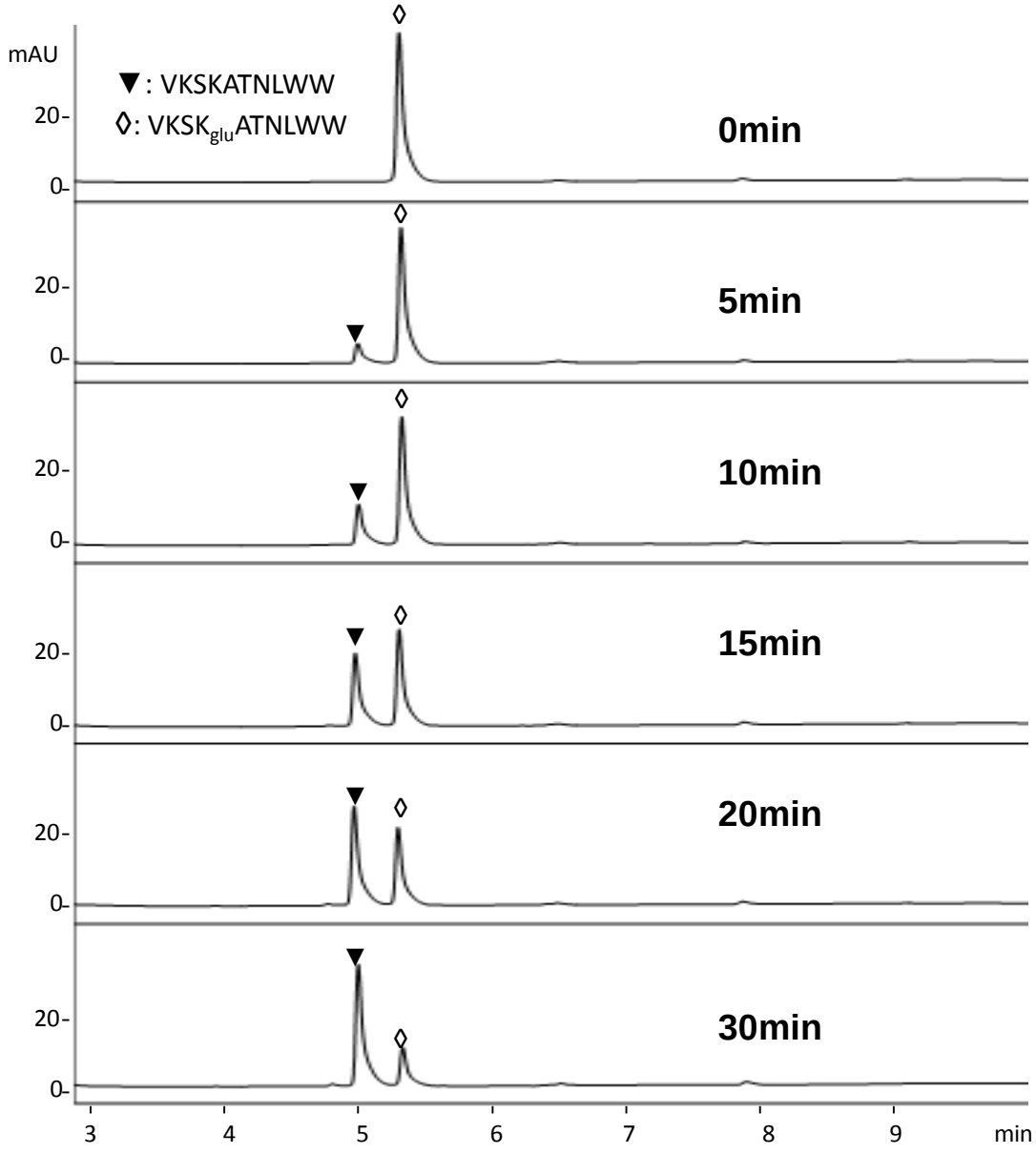

(E) Time course study of SIRT5's lysine deglutarylation activity: the enzymatic reactions were carried out at 37^{o}C for different durations and then deglutarylation products were detected by HPLC/MS.

Supplementary Figure S3F

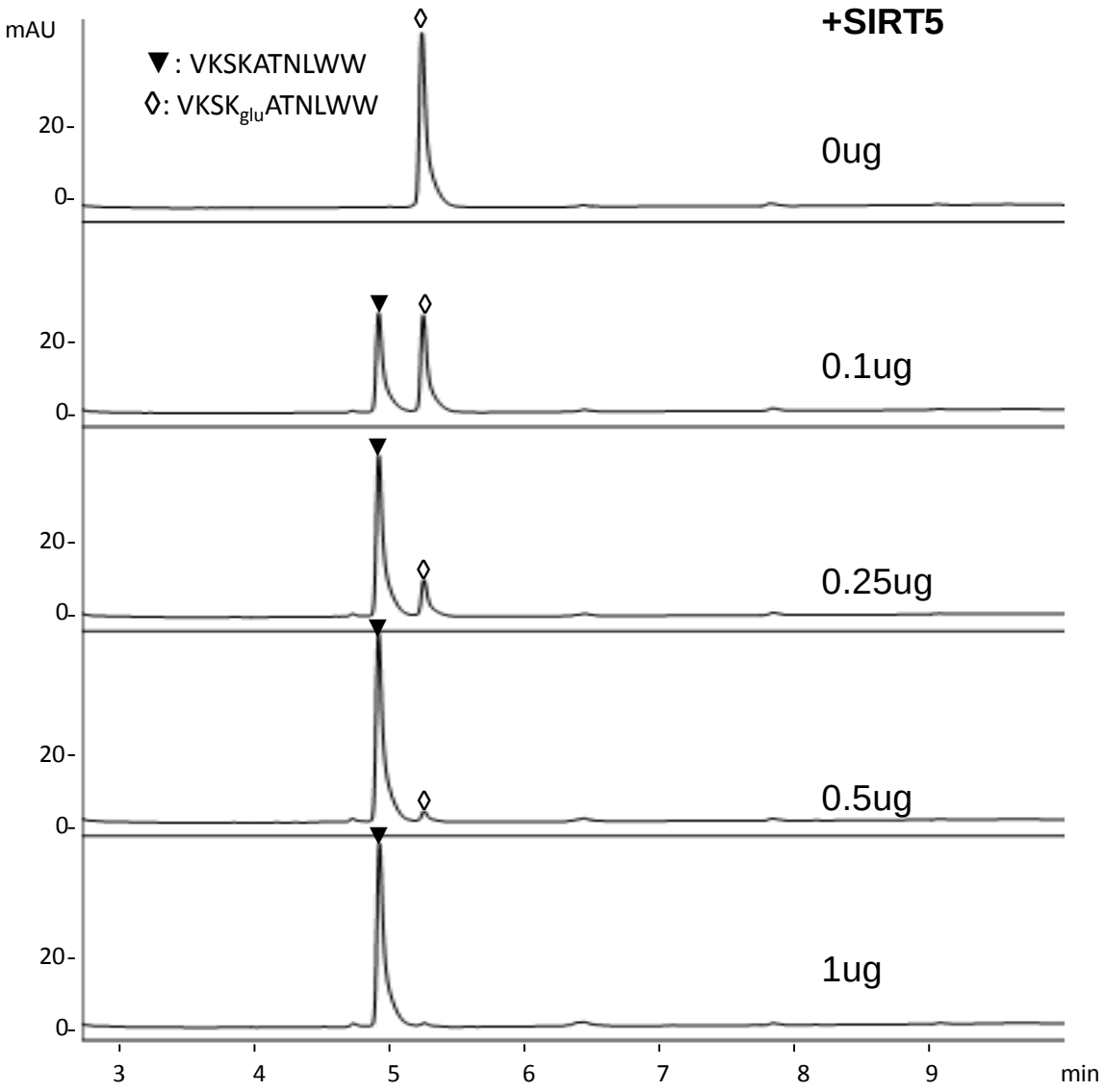

(F) Dosage of SIRT5 in lysine deglutarylation: enzymatic reactions were carried out with different amount of SIRT5 and then detected by HPLC/MS.

Supplementary Figure S3G

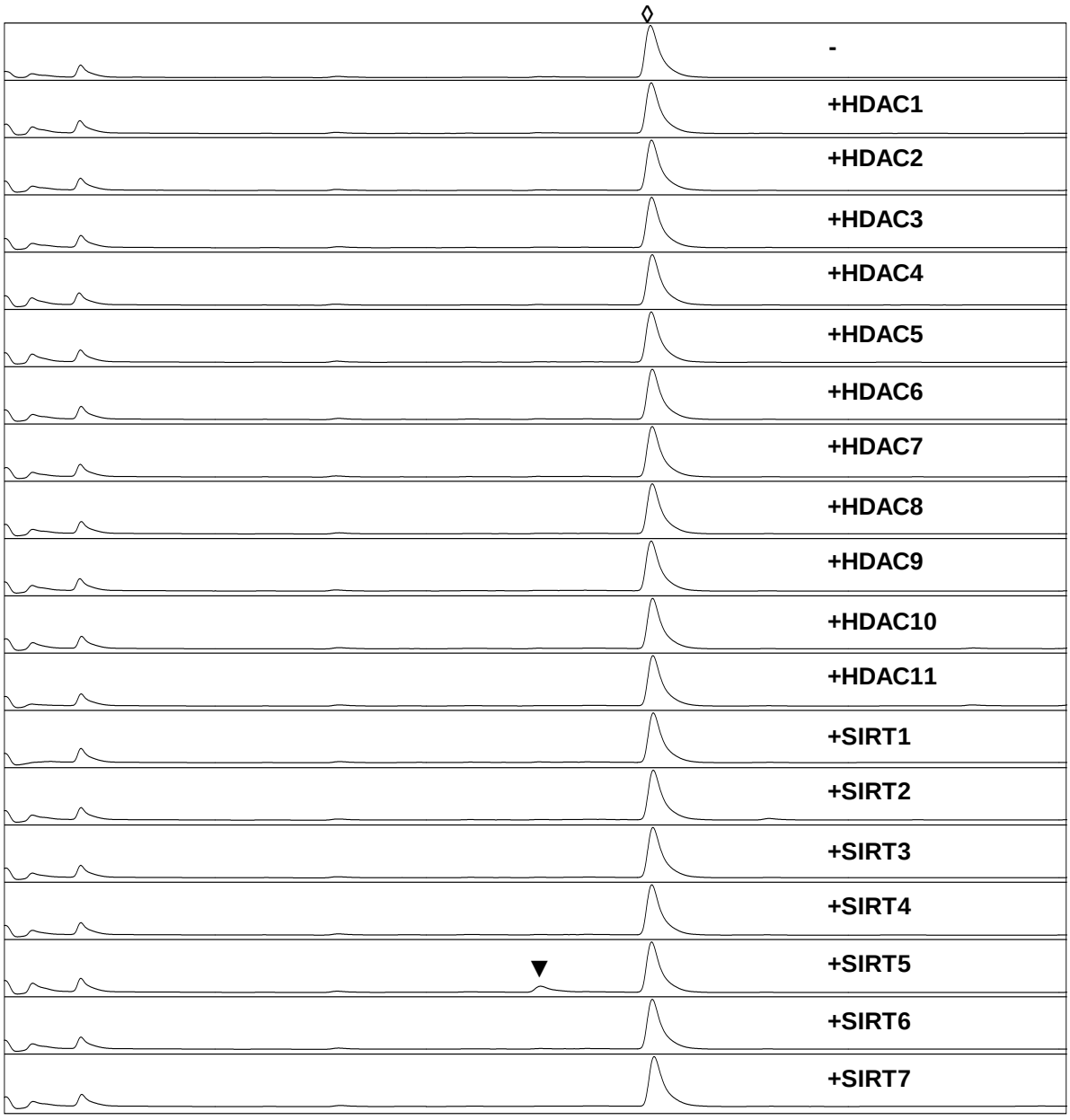

▼: VKSKATNLWW

◊: VKSK$_{glu}$ATNLWW

(G) HPLC trace of a glutarylated peptide, VKSK$_{glu}$ATNLWW (HRMS, m/z, 637.8480 Da, before and after *in vitro* deacylation reactions with HDAC1-11 and SIRT1-7.

Figure S4. Enzymology studies on SIRT5-catalyzed deglutarylation (related to Figure 4).

Supplementary Figure S4A

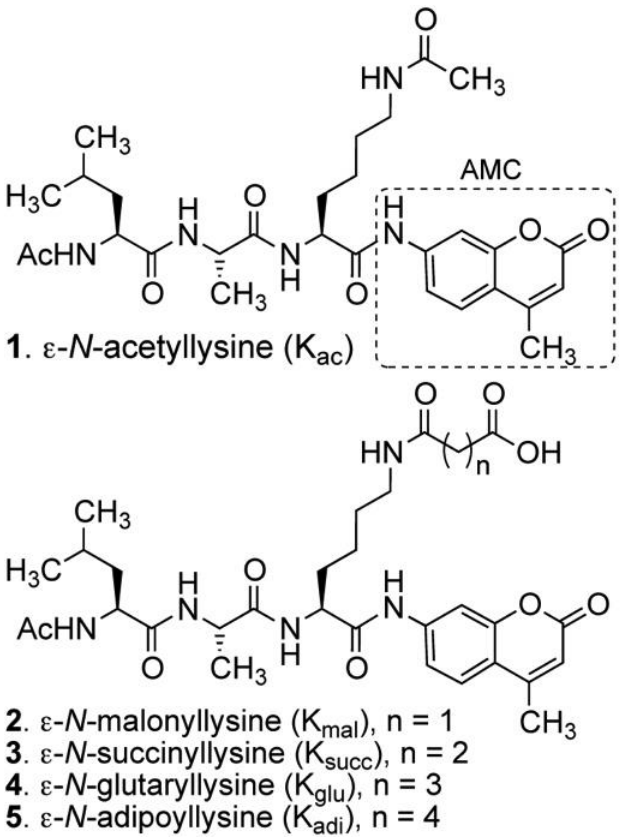

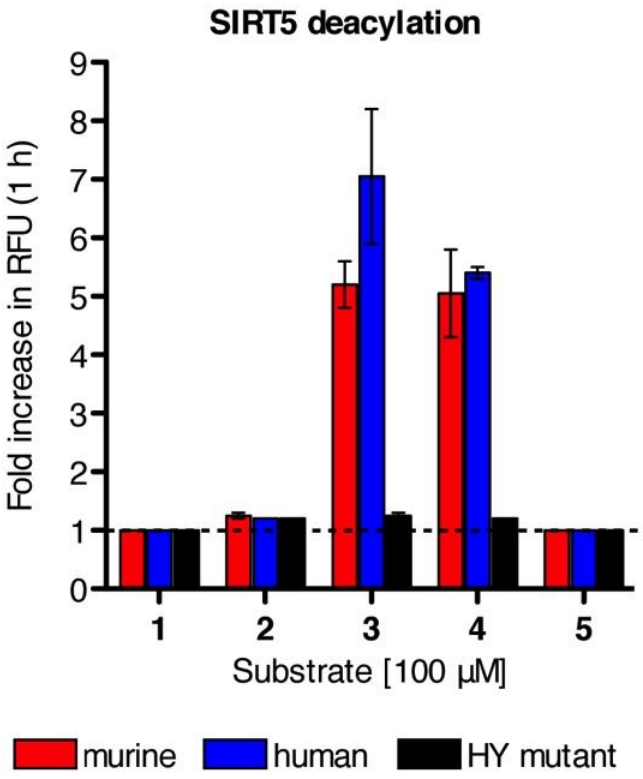

(A) Lysine side chains derivatized with dicarboxylic acids of varying lengths ranging from 3–6 carbon atoms (i.e., ε-*N*-malonyl-, ε-*N*-succinyl-, ε-*N*-glutaryl-, and ε-*N*-adipoyllysine) were generated. Two series of fluorogenic peptide substrates containing 7-amino-4-methylcoumarin (AMC) were evaluated; one series based on a simple α-*N*-acetylated lysine and one containing the tripeptide sequence, Ac-Leu-Gly-Lys(acyl) (data not shown). Endpoint deacylation assay of mouse or human wild-type SIRT5 or human mutant SIRT5 (HY mutant) against acylated mono-lysine-AMC substrates; K_{ac}, acetyl-lysine; K_{mal}, malonyl-lysine; K_{succ}, succinyl-lysine; K_{glu}, glutaryl-lysine; K_{adi}, adipoyl-lysine. Error bars represent SEM.

Supplementary Figure S4B

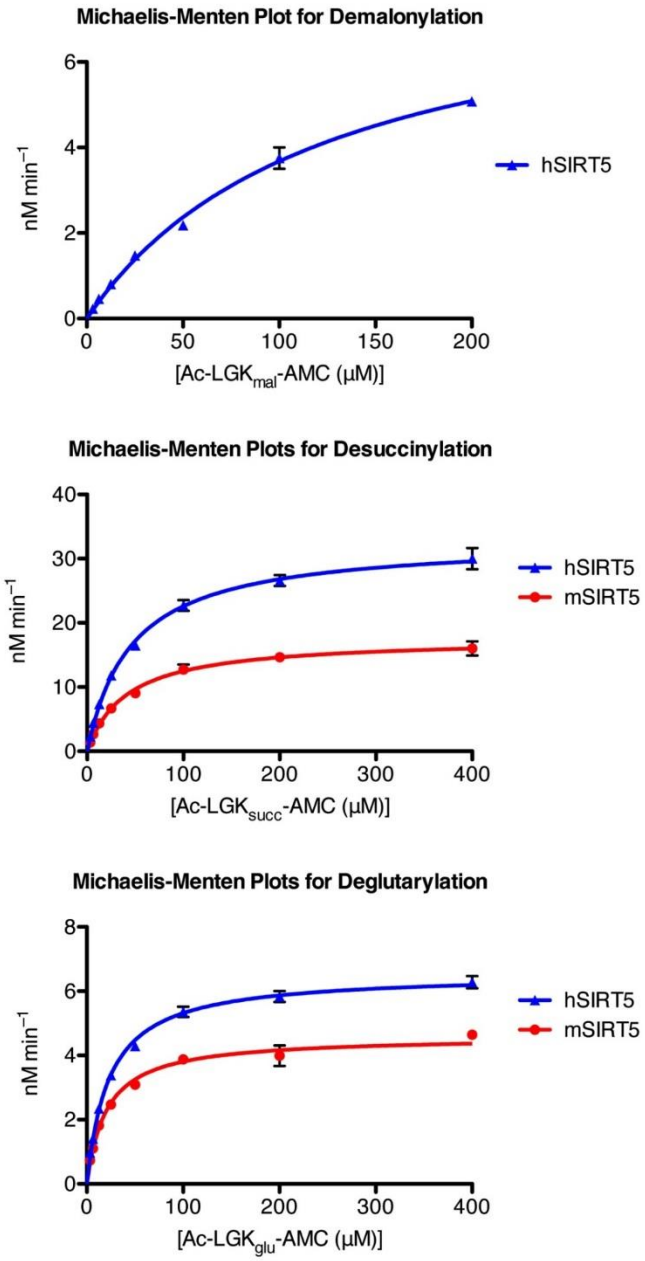

(B) Michaelis-Menten plots for substrates **2**–**4** using human SIRT5 (blue) and murine SIRT5 (red), respectively. The SIRT5 enzyme concentrations were 33 nM (1.0 ng × μL^{-1}) K_{succ} and K_{glu} substrates and 305 nM (9.3 ng × μL^{-1} for the K_{mal} substrate. Fluorescence readings were recorded every 30 seconds for at least 60 min at 25 ° C, to obtain initial linear rates **ν** (RFU min^{-1}) for each concentration. Error bars represent SEM.

Supplementary Figure S4C

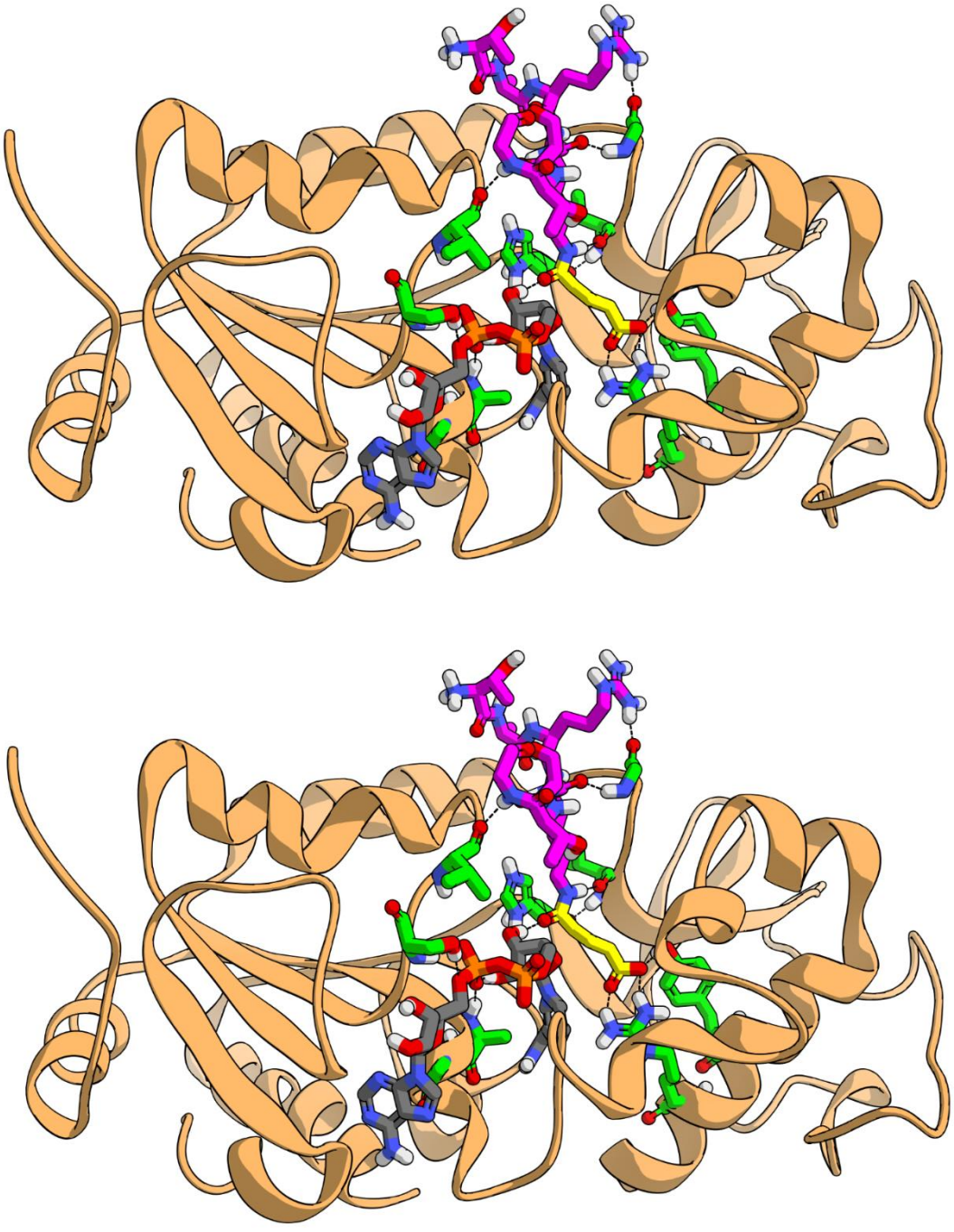

(C) Stereoview of the crystal structure of SIRT5 with a glutarylated peptide superimposed in the catalytic pocket.

Supplementary Figure S4D

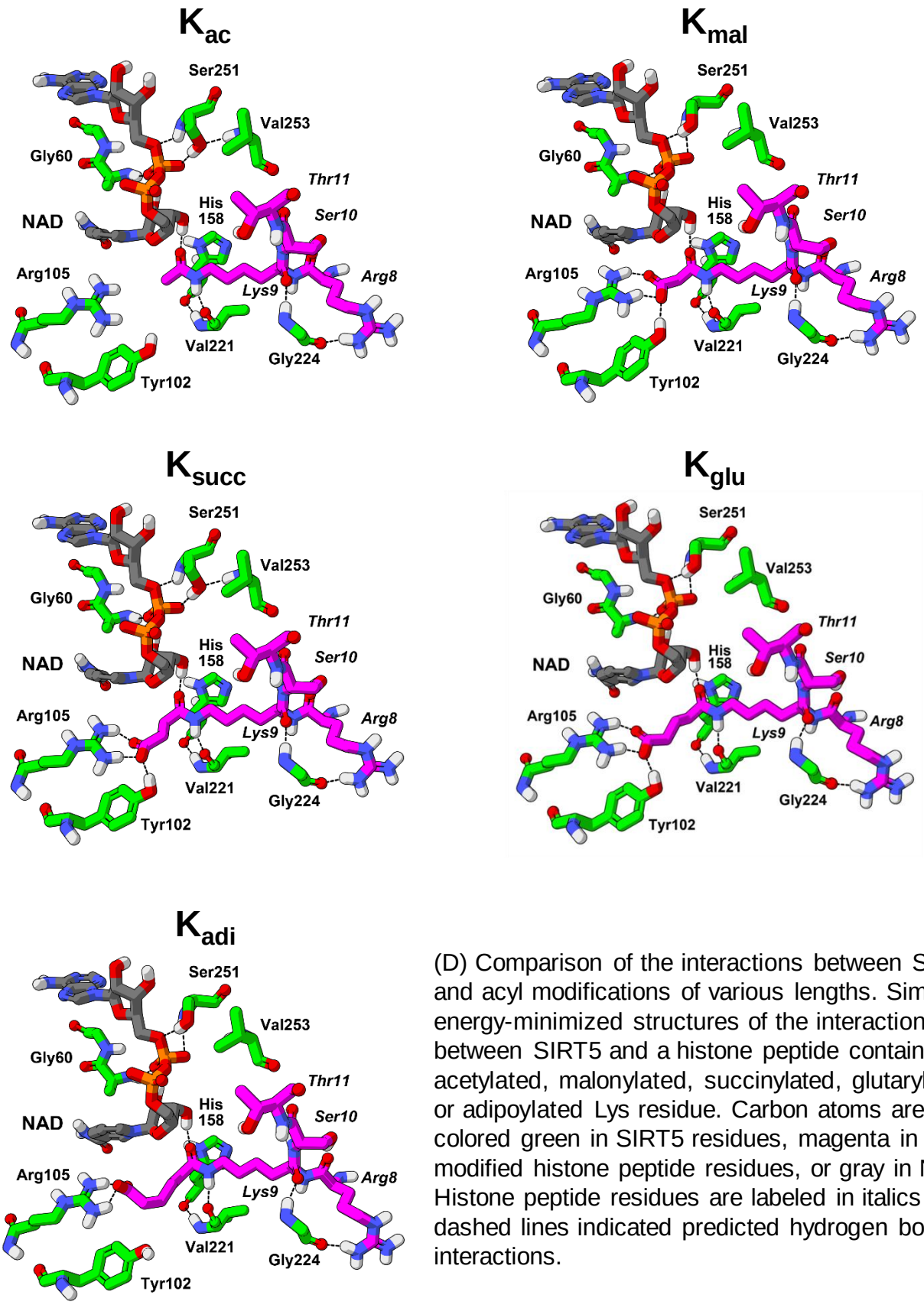

(D) Comparison of the interactions between SIRT5 and acyl modifications of various lengths. Simplified energy-minimized structures of the interactions between SIRT5 and a histone peptide containing an acetylated, malonylated, succinylated, glutarylated, or adipoylated Lys residue. Carbon atoms are colored green in SIRT5 residues, magenta in the modified histone peptide residues, or gray in NAD^+. Histone peptide residues are labeled in italics and dashed lines indicated predicted hydrogen bond interactions.

Supplementary Figure S4E

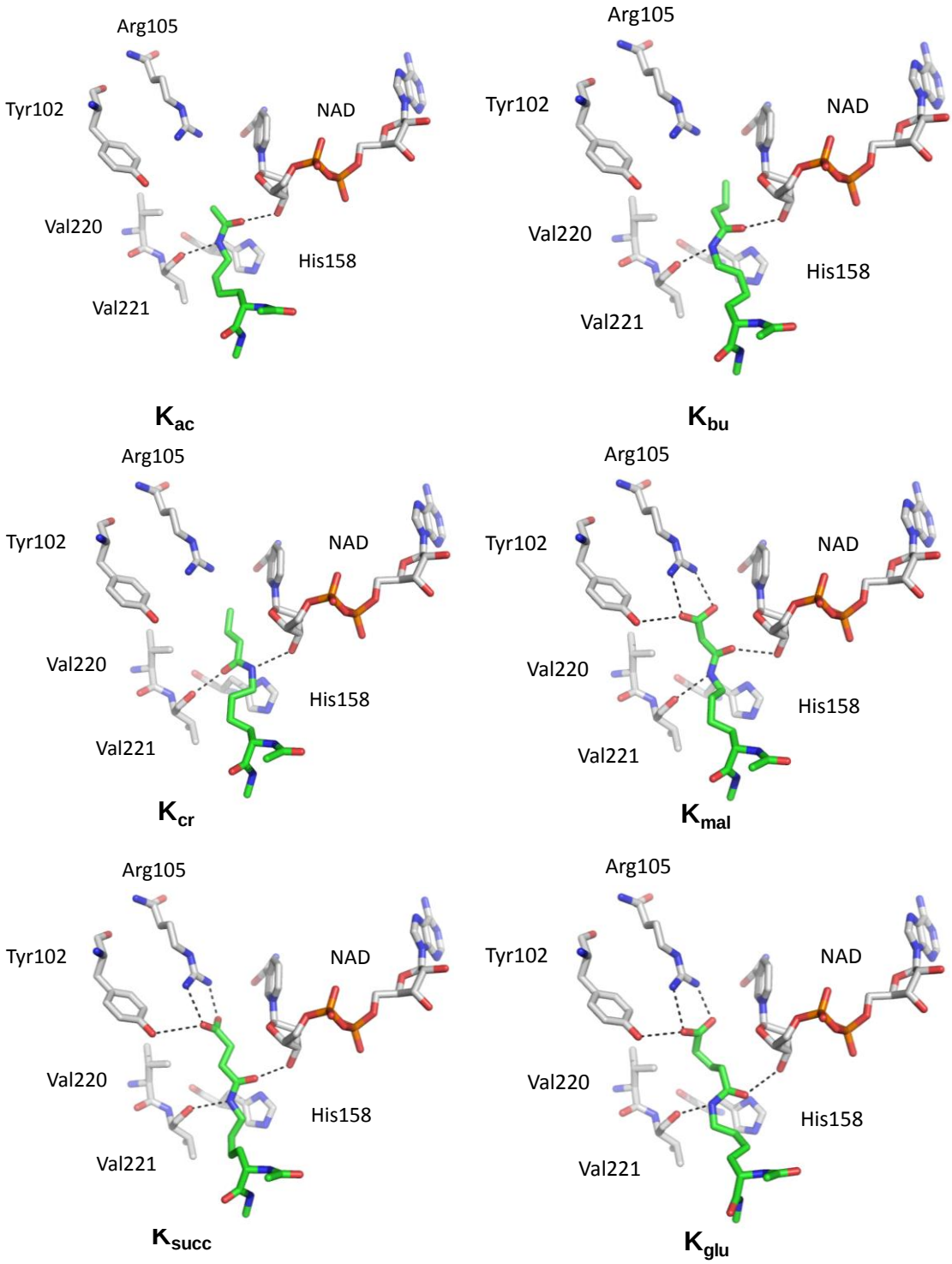

(E) Structural simulation of SIRT5 with acyl lysine residues using AutoDock software (v 4.2). Binding conformations of five acyl lysine residues, lysine acetylation (K_{ac}), butyrylation (K_{bu}), crotonylation (K_{cr}), succinylation (K_{succ}), malonylation (K_{mal}) and glutarylation (K_{glu}), to SIRT5 were analyzed.

Figure S5. Proteomic and bioinformatic analyses of K_{glu} substrates in SIRT5KO mouse liver (related to Figure 5).

Supplementary Figure S5A

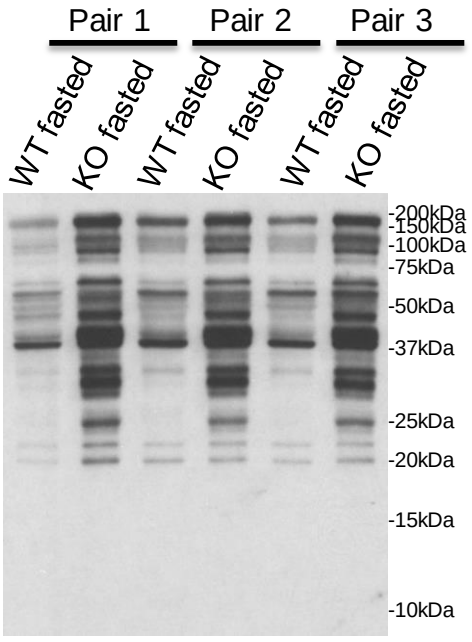

Anti-K_{succ}

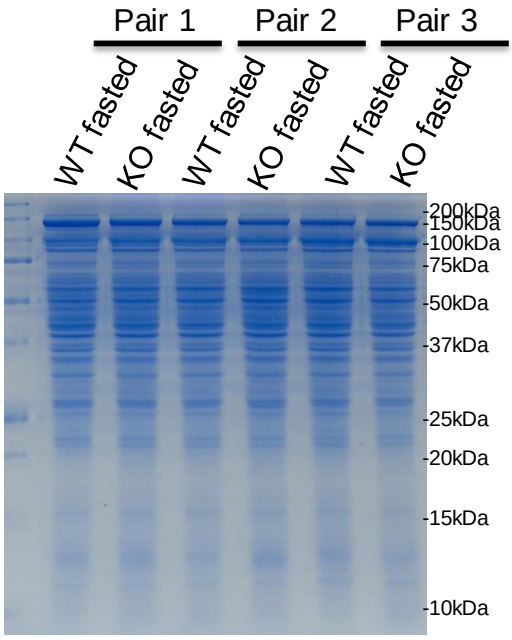

Coomassie Blue

(A) Western blotting analysis of mitochondria from *Sirt5*$^{+/+}$ (WT) and *Sirt5*$^{-/-}$ (KO) mouse livers. "WT" and "KO" represent SIRT5 WT and KO mice, respectively. The mitochondria were isolated from WT and SIRT5 KO 48h-fasted mice, and dissolved in SDS sample buffer. Western blotting analysis of mitochondrial protein lysates from WT and SIRT5 KO 48h-fasted mouse livers. The samples were subjected to SDS-PAGE. Western blotting analysis on the samples with anti-K_{succ} antibody.

Supplementary Figure S5B

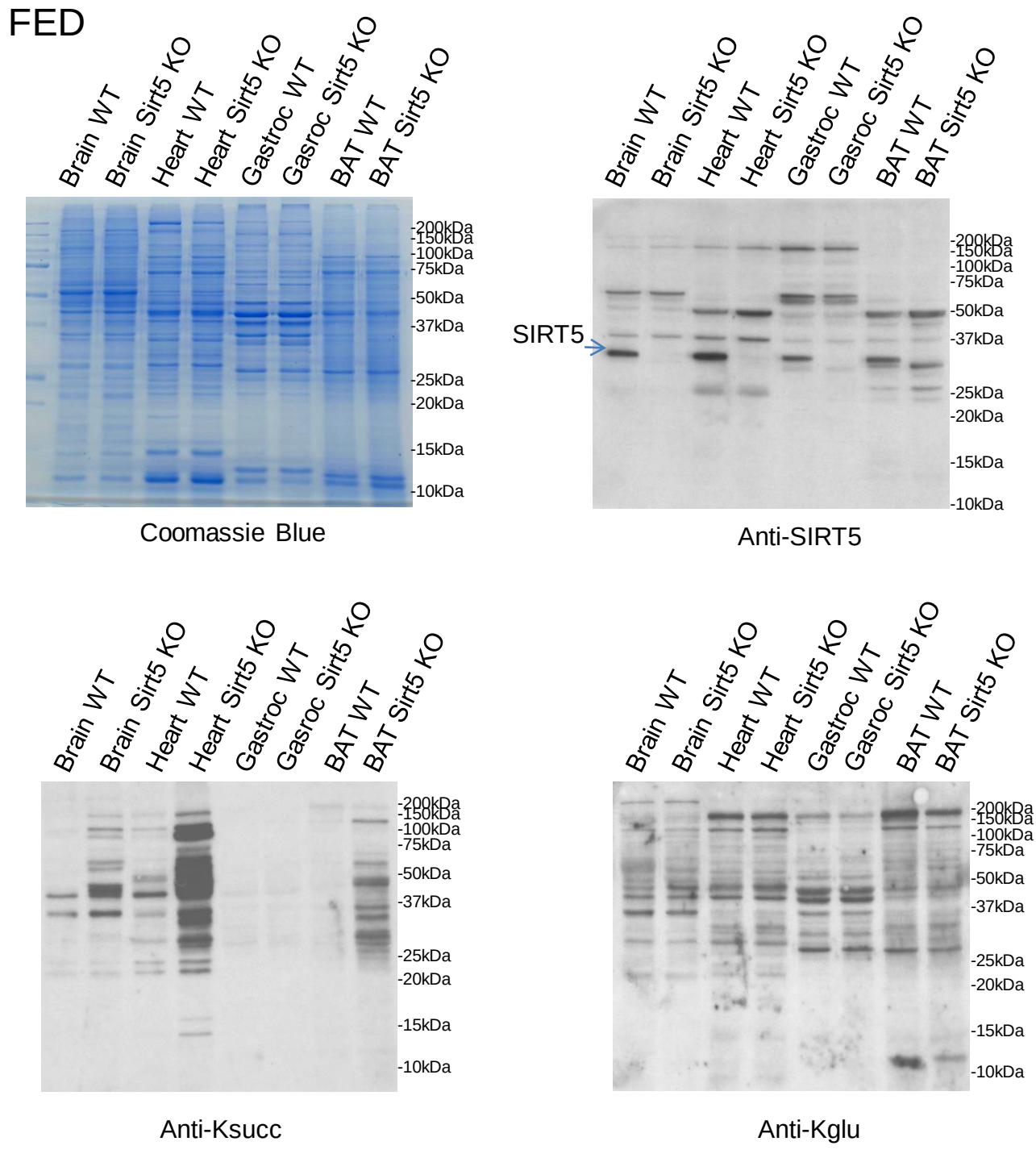

(B) Western blotting analysis was performed on mitochondrial lysates from mouse brain, heart, gastrocnemius (gastroc) and brown adipose (BAT) tissues in the fed state.

Supplementary Figure S5C

FASTED

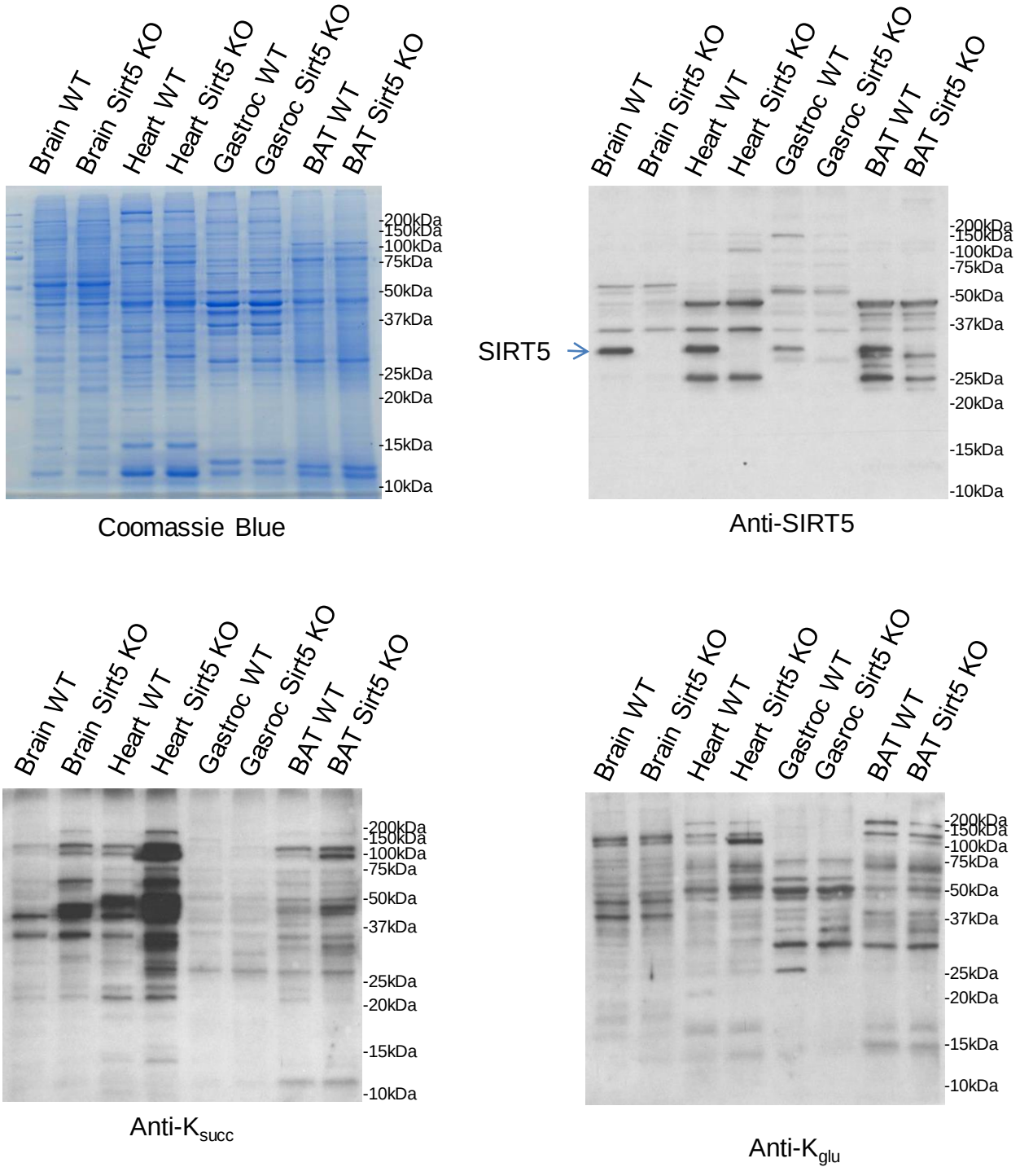

(C) Western blotting analysis was performed on mitochondrial lysates from mouse brain, heart, gastrocnemius (gastroc) and brown adipose (BAT) tissues in the fasted state.

Supplementary Figure S5D

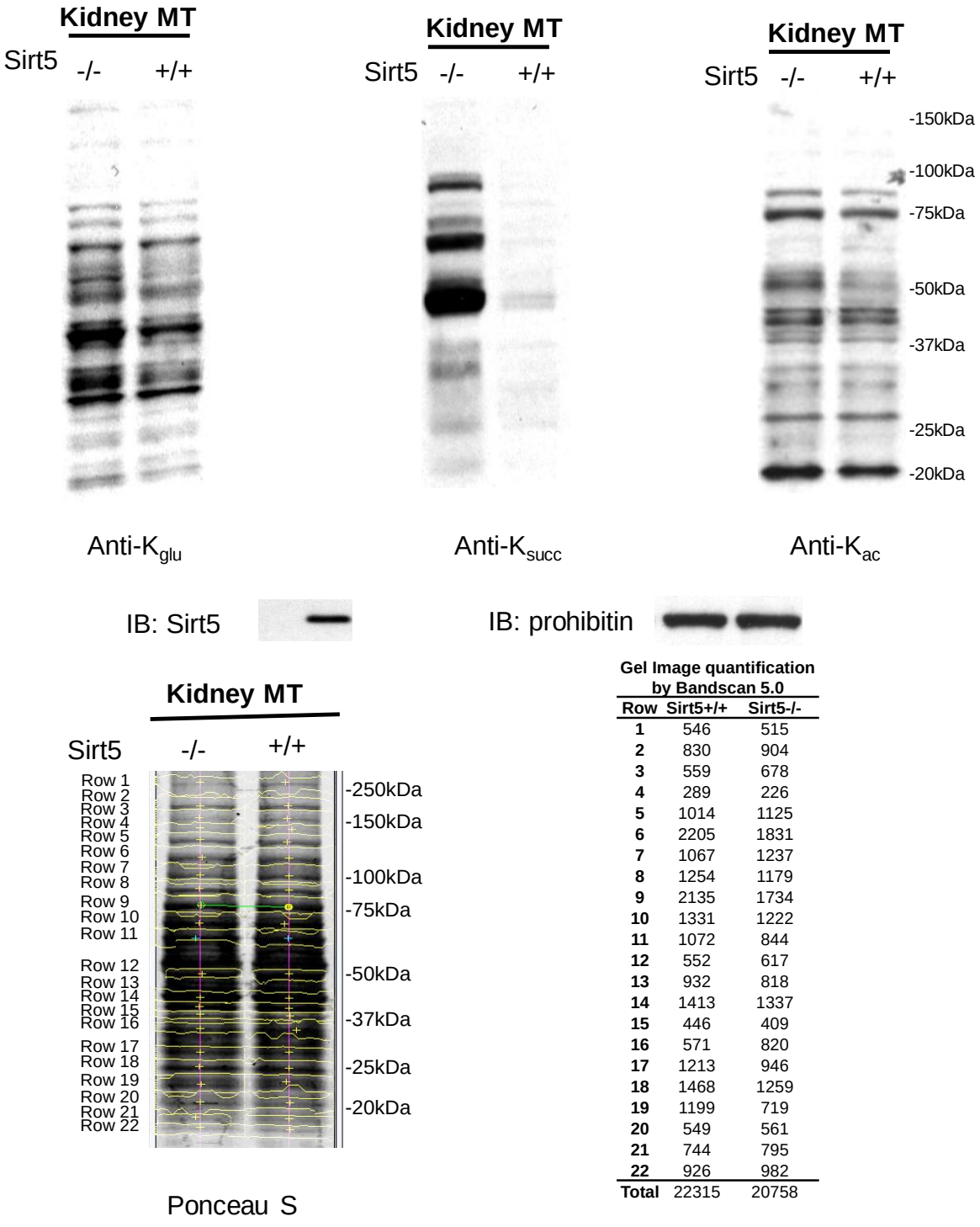

Gel Image quantification by Bandscan 5.0

Row	Sirt5+/+	Sirt5-/-
1	546	515
2	830	904
3	559	678
4	289	226
5	1014	1125
6	2205	1831
7	1067	1237
8	1254	1179
9	2135	1734
10	1331	1222
11	1072	844
12	552	617
13	932	818
14	1413	1337
15	446	409
16	571	820
17	1213	946
18	1468	1259
19	1199	719
20	549	561
21	744	795
22	926	982
Total	22315	20758

(D) Western blotting analysis of mitochondrial lysates from WT and SIRT5 KO mouse kidneys. Thirty μg of mouse kidney mitochondrial protein lysates were used for the analysis anti-K_{glu}, anti-K_{succ} and anti-K_{ac} antibodies were performed from the mitochondrial lysates of the same WT or SIRT5 KO mouse Kidney. The Ponceau S loading control were quantified from the integration of the band image intensity by Bandscan 5.0, showing that the loading of samples are almost equal.

Supplementary Figure S5E

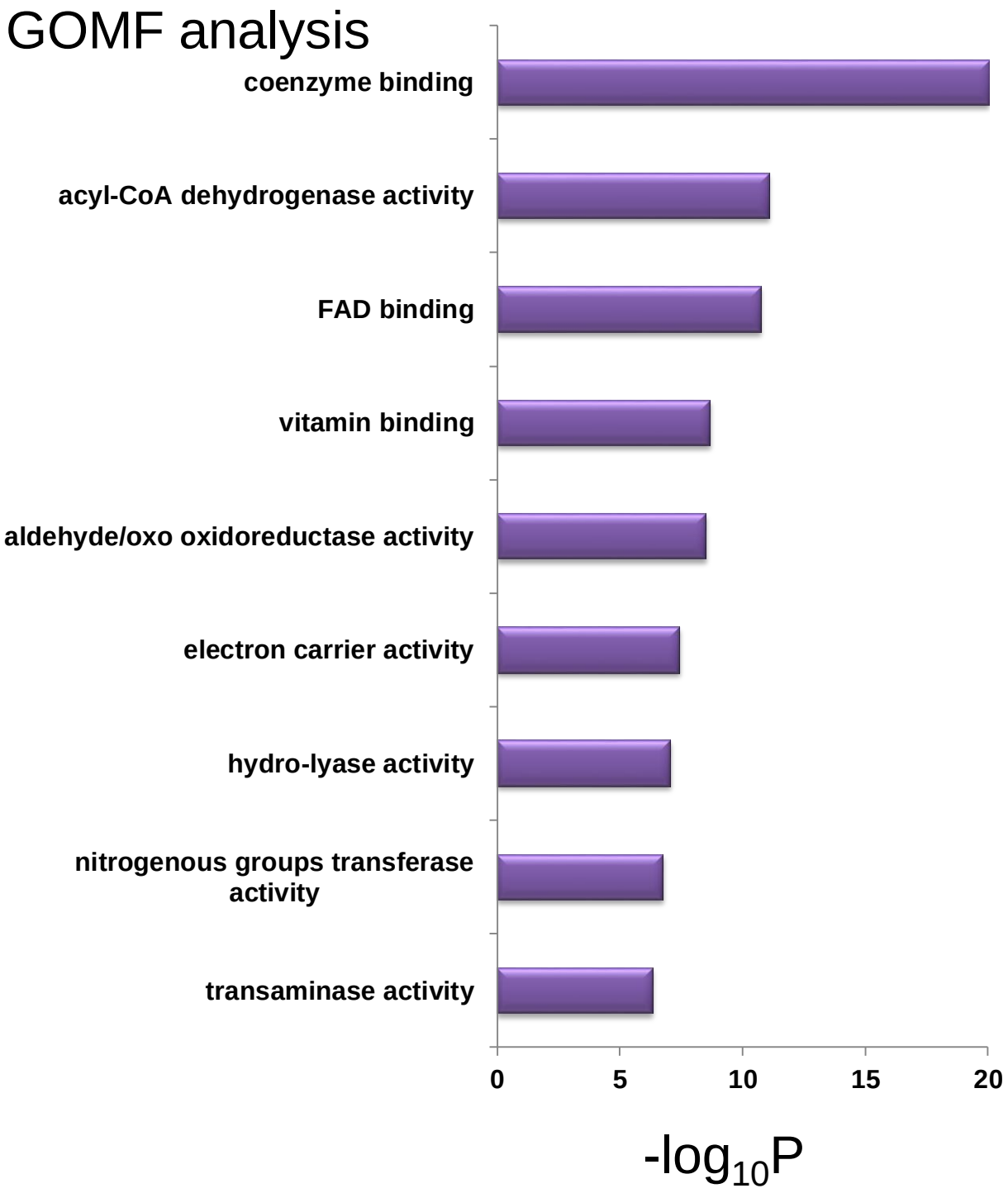

(E) Functional annotation and enrichment analysis of K_{glu} substrates by analyzing gene ontology molecular functions.

Supplementary Figure S5F

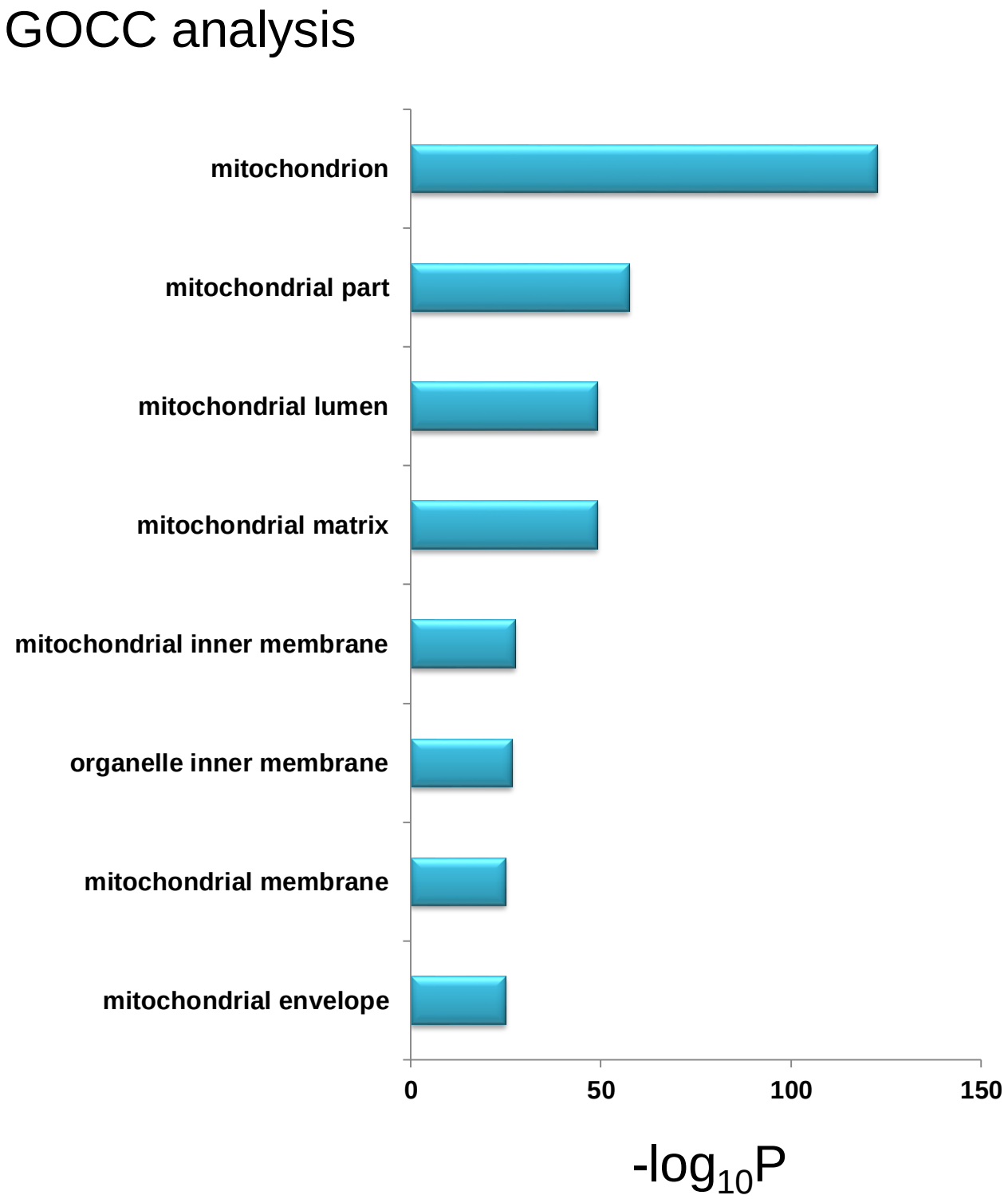

(F) Functional annotation and enrichment analysis of K_{glu} substrates by analyzing gene ontology cellular compartments.

Supplementary Figure S5G

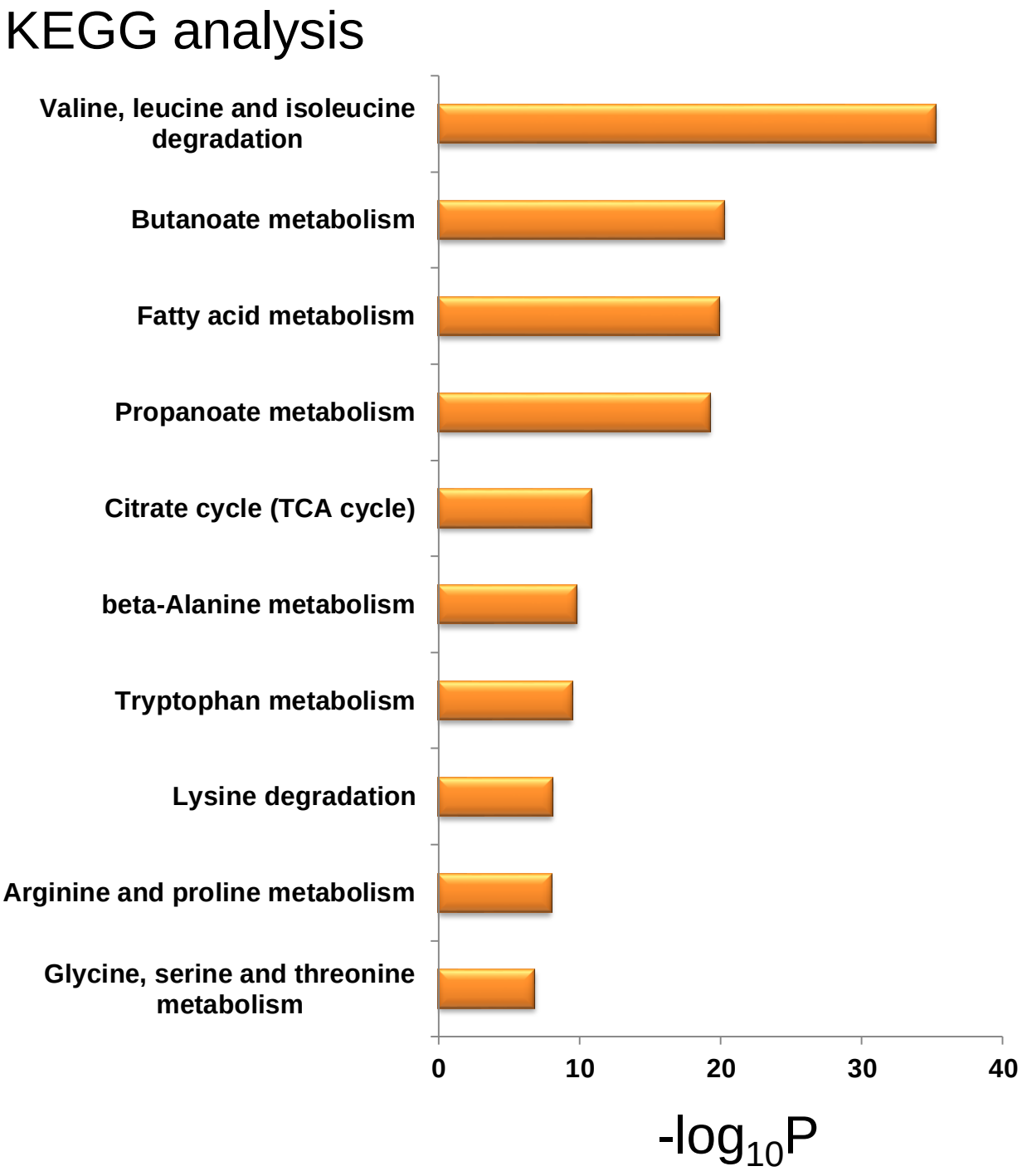

(G) Functional annotation and enrichment analysis of K_{glu} substrates by analyzing KEGG metabolic pathways. IPI IDs of Kglu proteins enriched in each pathway are listed in Supplemental Table S4D.

Supplementary Figure S5H

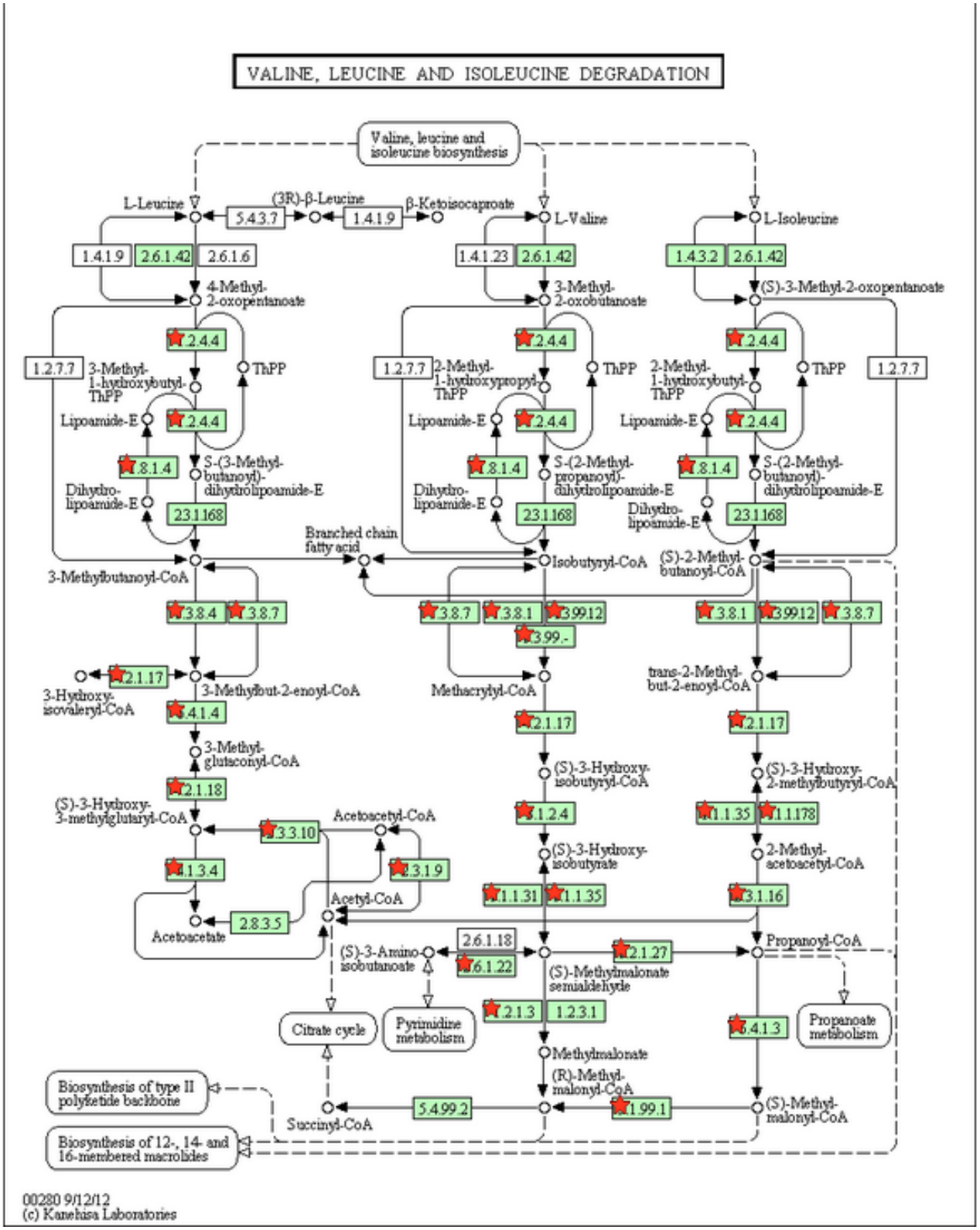

(H) Illustration of enriched KEGG pathways of K_{glu} proteins in valine, leucine and isoleucine degradation. The K_{glu} proteins are indicated by a red star. IPI IDs of the K_{glu} proteins are listed in Supplemental Table S4D.

Supplementary Figure S5I

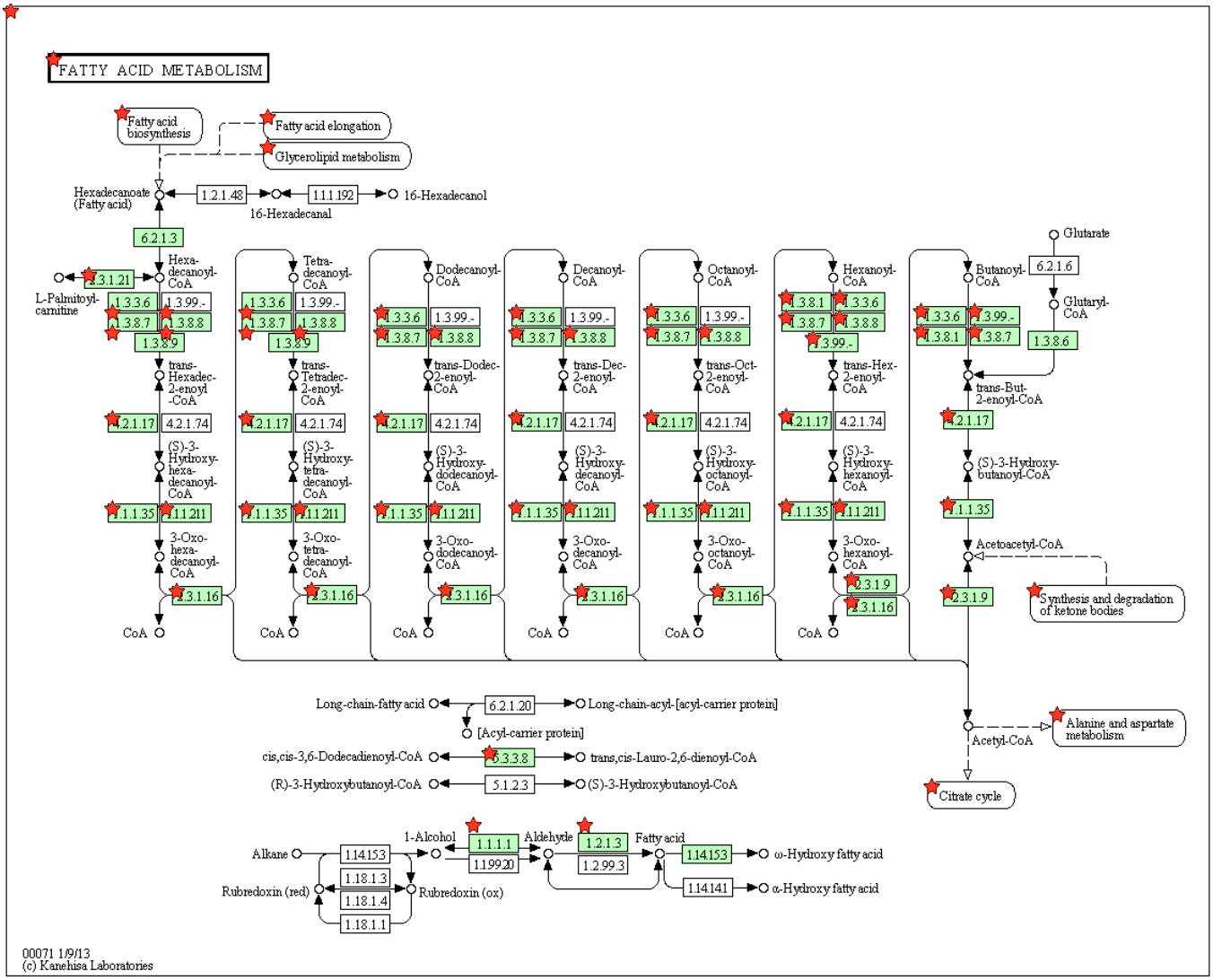

(I) Illustration of enriched KEGG pathways of K_{glu} proteins in fatty acid metabolism. IPI IDs of the K_{glu} proteins are listed in Supplemental Table S4D.

Supplementary Figure S5J

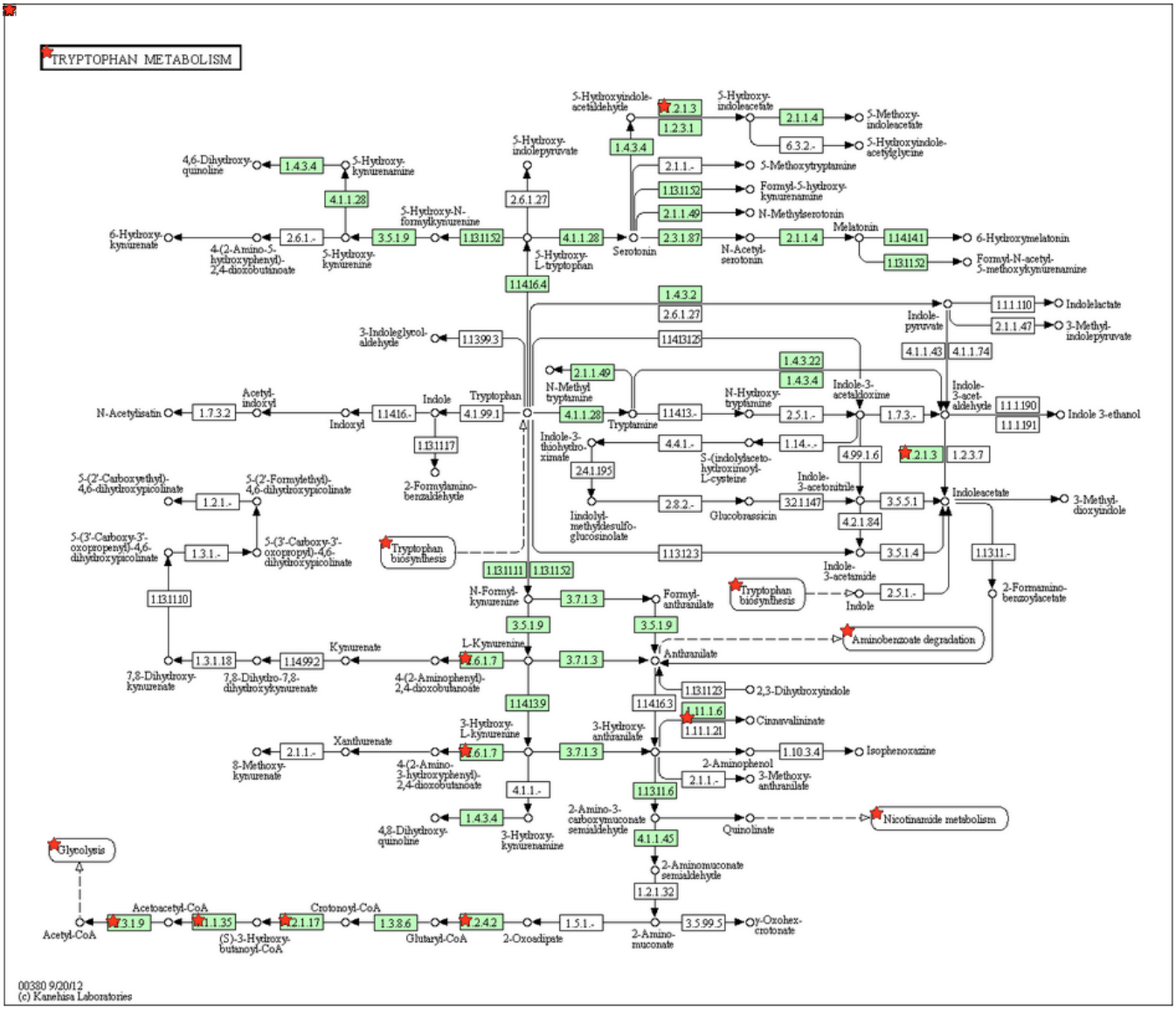

(J) Illustration of enriched KEGG pathways of K_{glu} proteins in tryptophan metabolism. IPI IDs of the K_{glu} proteins are listed in Supplemental Table S4D.

Supplementary Figure S5K

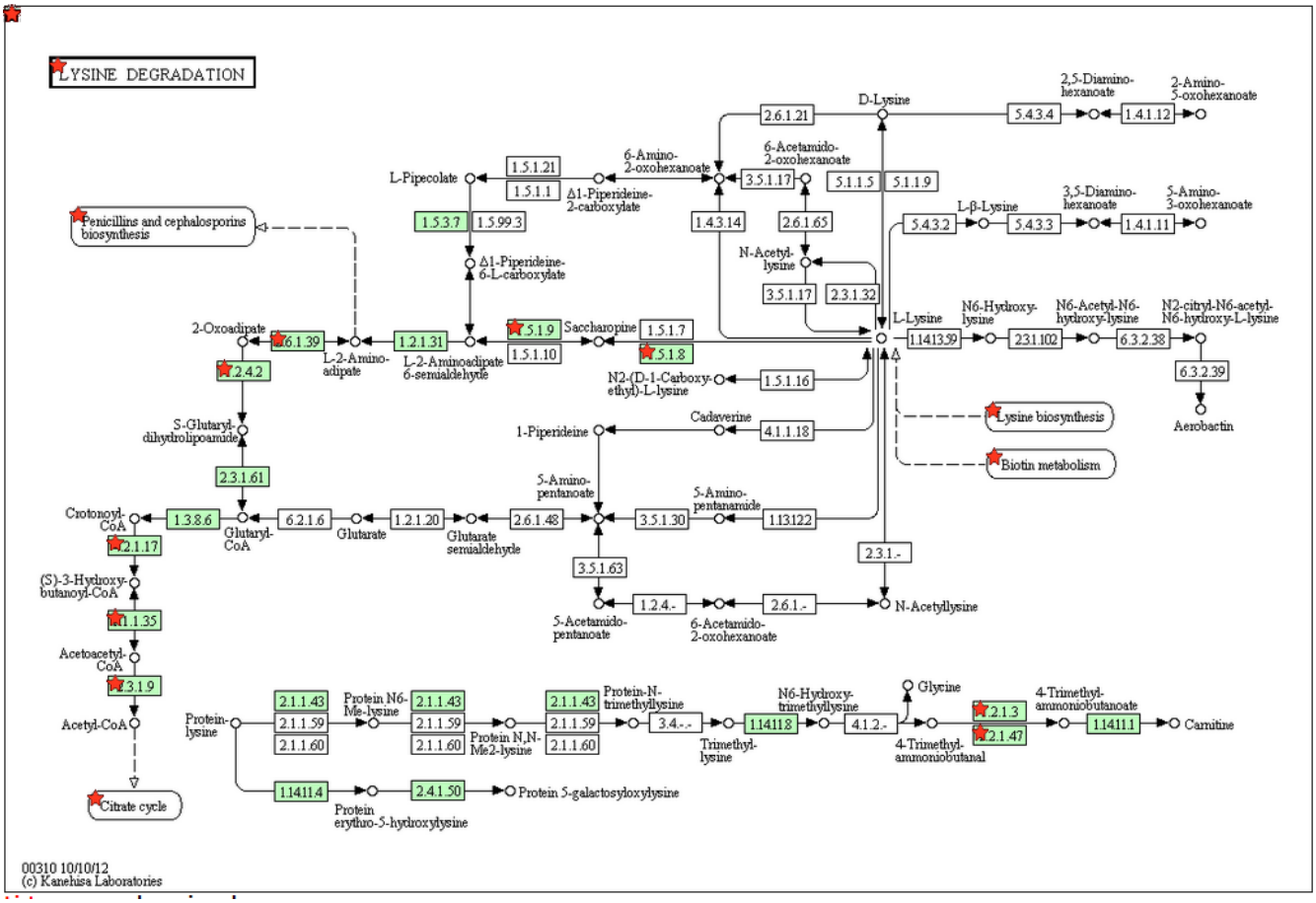

(K) Illustration of enriched KEGG pathways of K_{glu} proteins in lysine degradation. IPI IDs of the K_{glu} proteins are listed in Supplemental Table S4D.

Supplementary Figure S5L

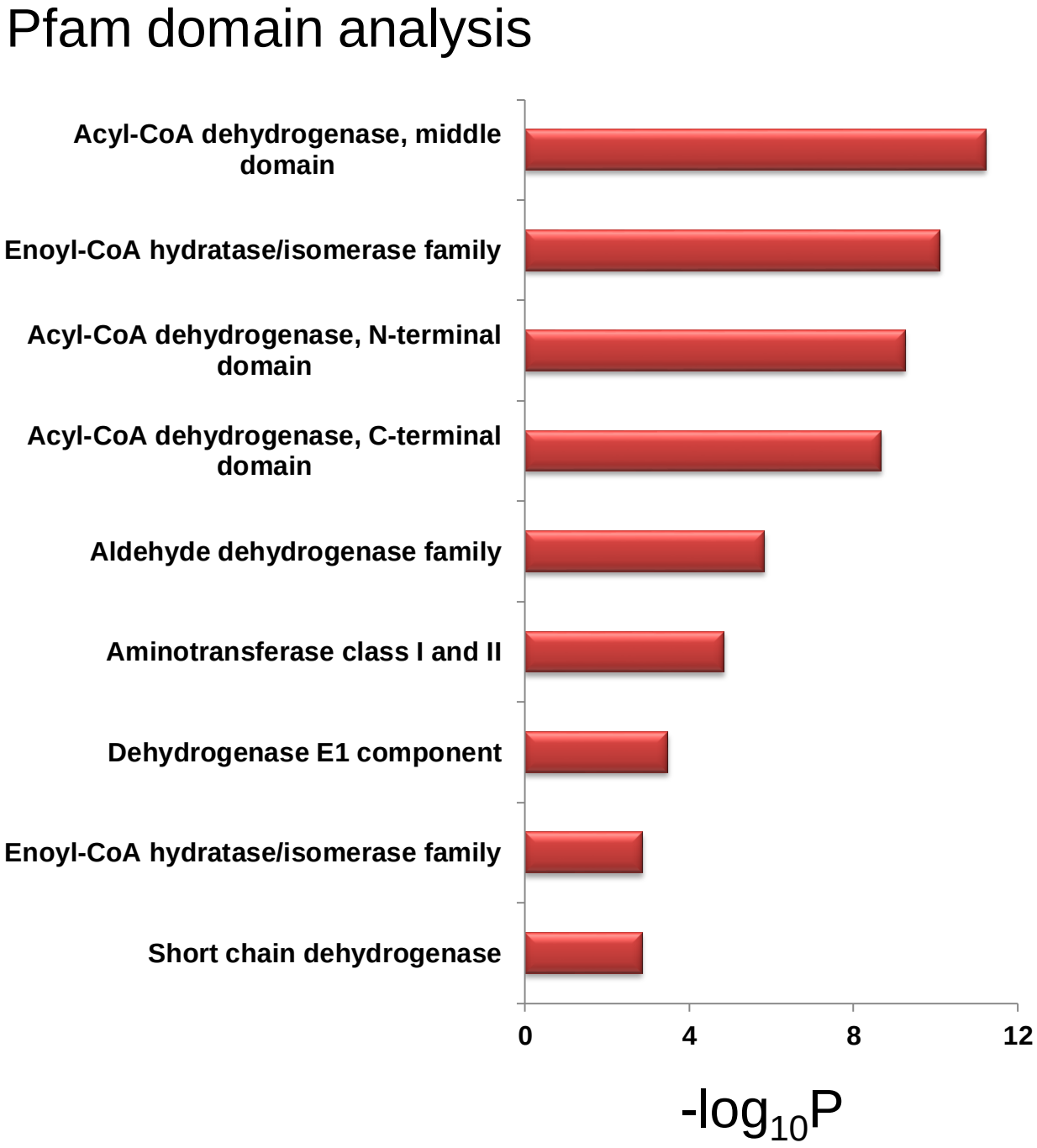

(L) Enriched domains of K_{glu} proteins from Pfam database.

Supplementary Figure S5M

Enriched protein complexes of K_{glu} proteins from CORUM database.

Complex name	Synonyms	Adjusted P_value
F1F0-ATP synthase (EC 3.6.3.14), mitochondrial	Complex V | F1F0 ATPase	3.8×10^{-8}
Respiratory chain complex I, mitochondrial	NADH dehydrogenase (EC 1.6.5.3)	4.0×10^{-3}

Supplementary Figure S5N

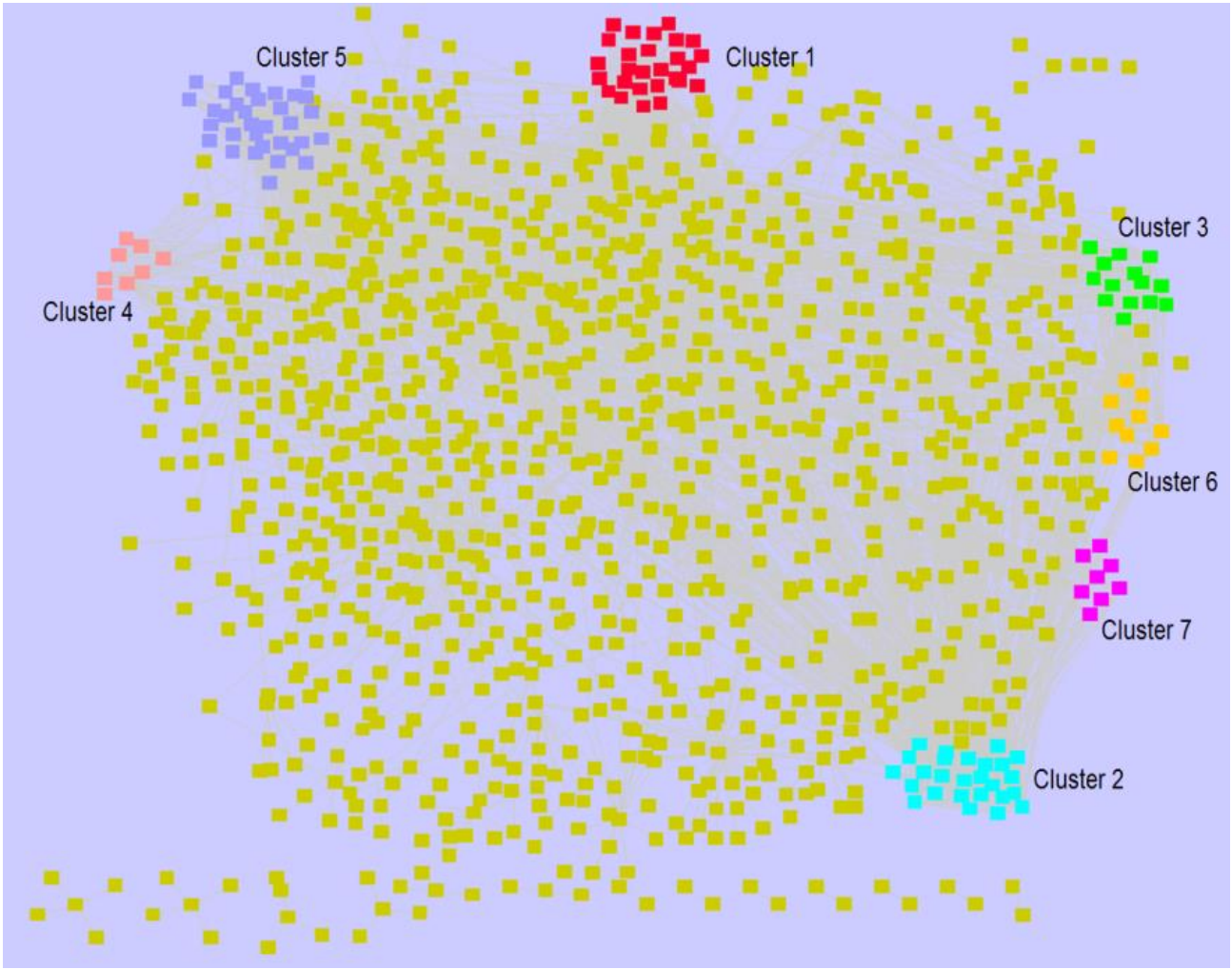

(N) Interaction network of K_{glu} proteins and their interacting proteins obtained from STRING 9.0 database and visualized in Cytoscape (1,149 of nodes and 5,532 edges). Top 7 most highly ranked clusters are marked in different colors.

Supplementary Figure S5O

Cluster 1 (MCODE score = 8.889)
nodes = 27 , edges = 240

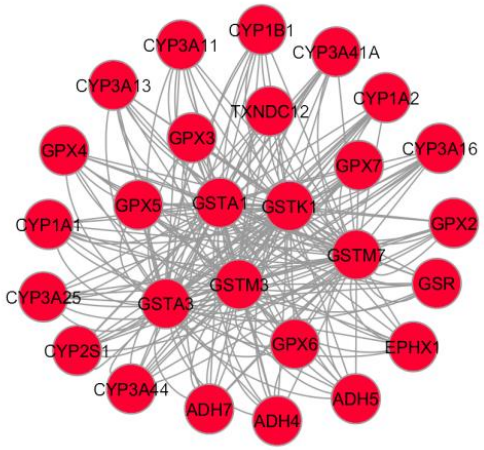

Cluster 2 (MCODE score = 8.462)
nodes = 26 , edges = 220

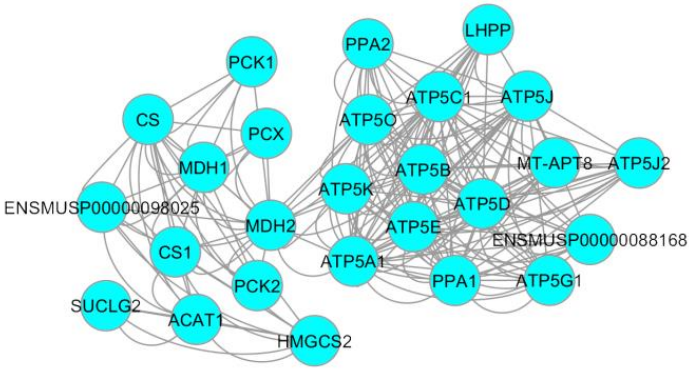

Cluster 3 (MCODE score = 5.571)
nodes = 14 , edges = 78

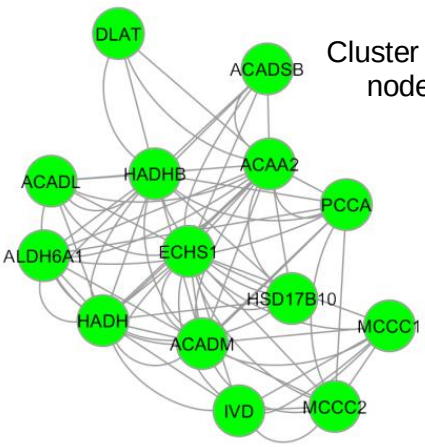

Cluster 4 (MCODE score = 4.5)
nodes = 8 , edges = 36

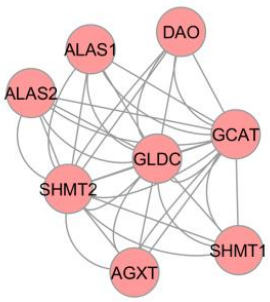

Cluster 5 (MCODE score = 3.515)
nodes = 33 , edges = 116

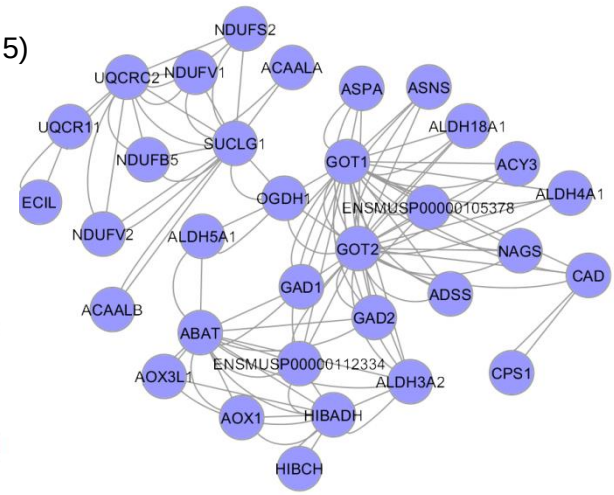

Cluster 6 (MCODE score = 3.2)
nodes = 10 , edges = 32

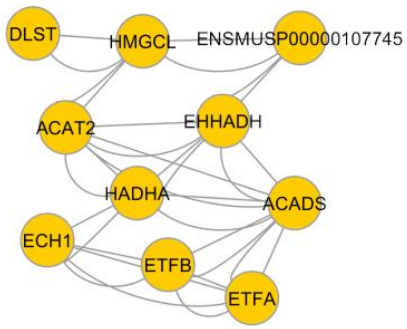

Cluster 7 (MCODE score = 2)
nodes = 8 , edges = 16

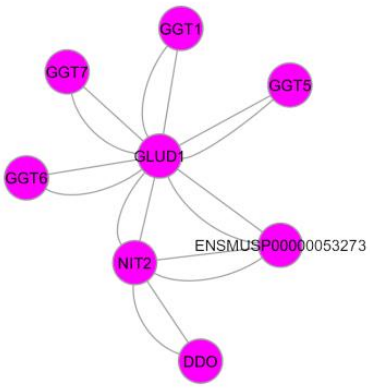

(O) Top 7 most highly ranked and tightly connected network clusters from (N) of K_{glu} by MCODE analysis.

Figure S6. Carbamoyl Phosphate Synthase 1 is targeted for deglutarylation by SIRT5 (related to Figure 6).

Supplementary Figure S6A

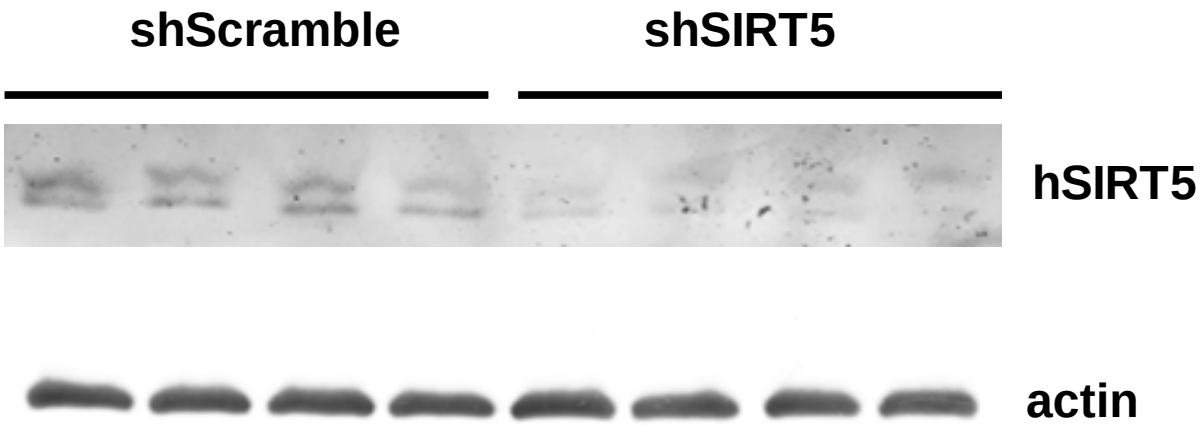

(A) HeLa cells containing a shScramble (SCR) or shSIRT5 were measured for SIRT5 levels using an anti-SIRT5 antibody.

Supplementary Figure S6B

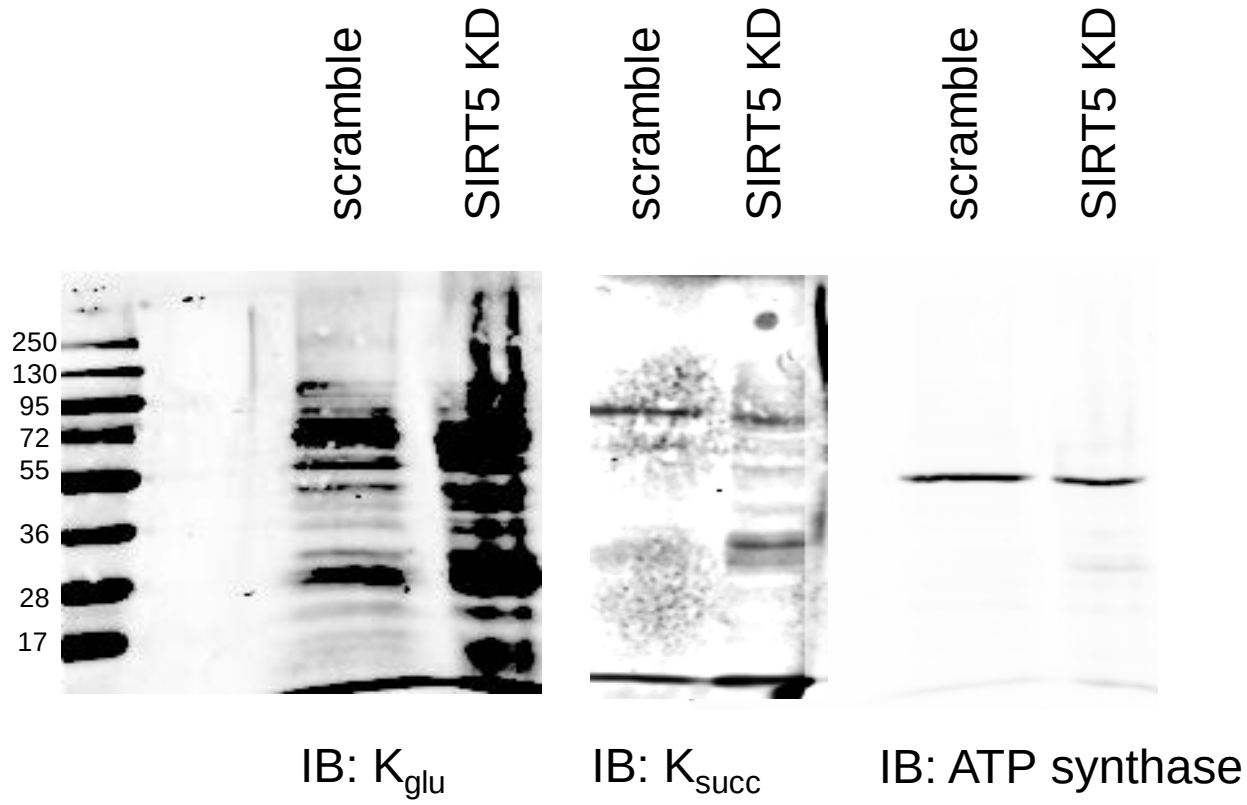

(B) HEK293 cells containing a shScramble (SCR) or shSIRT5 were measured for protein glutarylation levels using an anti-K_{glu} antibody, protein succinylation using an anti-K_{succ} antibody, and normalized to protein content using an anti-ATP-synthase antibody.

Figure S7. Physiology and pathophysiology of lysine glutarylation (related to Figure 7).

Supplementary Figure S7A

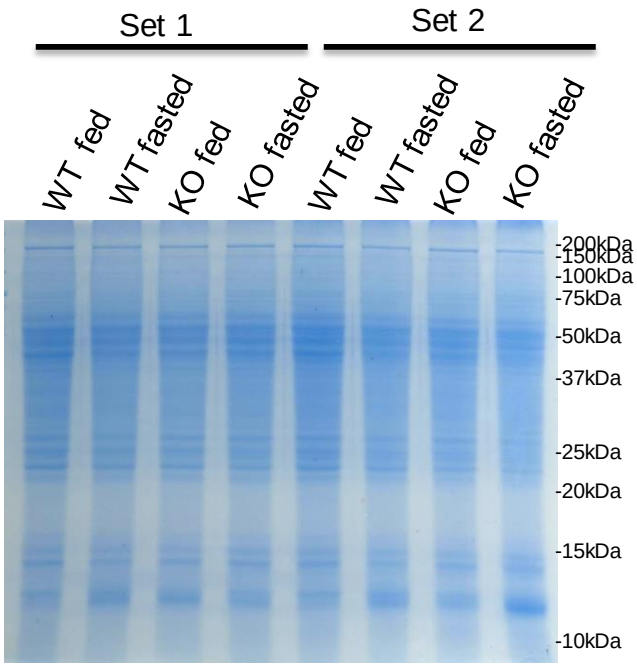

Coomassie Blue

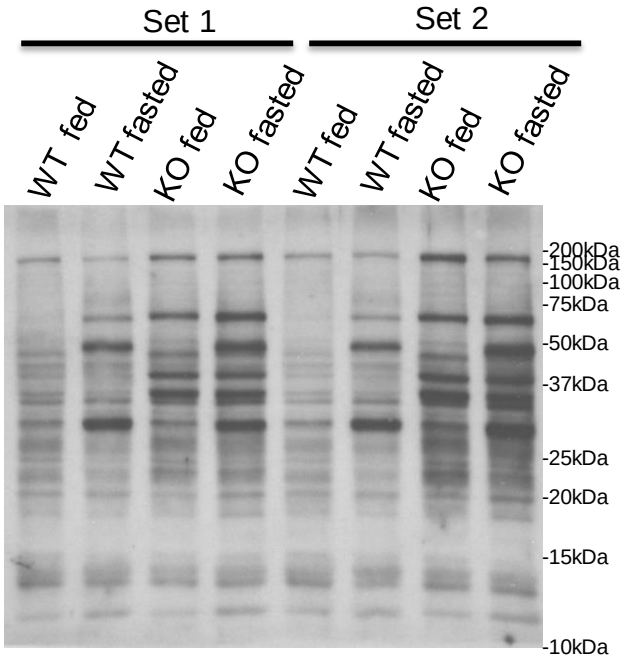

Anti-K_{succ}

(A) Hepatic whole-cell protein succinylation was measured by immunoblotting with an anti-K_{glu} antibody in two sets (Set1 and Set2) of SIRT5 WT and KO mouse livers that were fed or fasted (48h), respectively. Lysate samples were dissolved in SDS sample buffer and subjected to SDS-PAGE for measurement of protein succinylation using an anti-K_{succ} antibody.

Supplementary Figure S7B

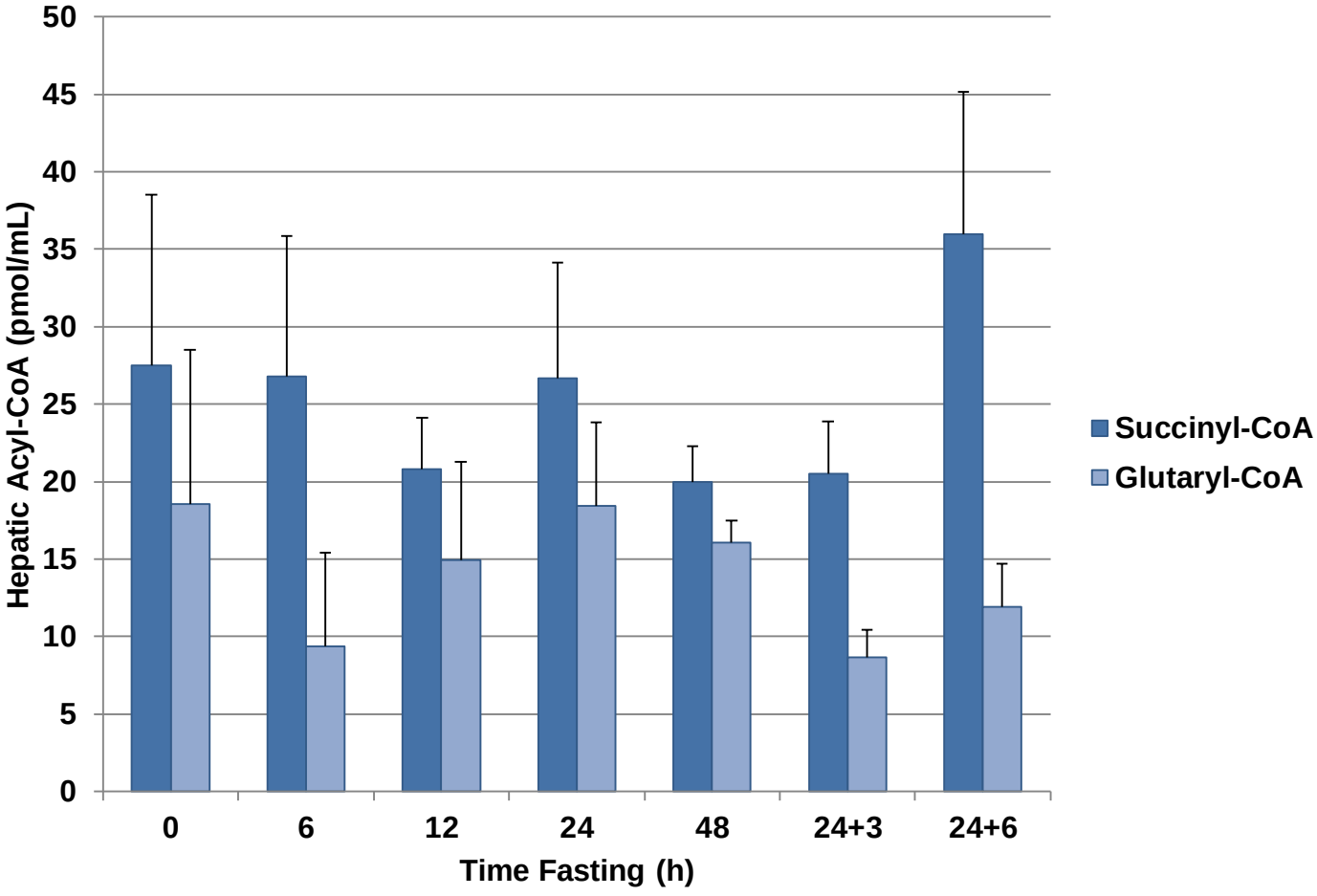

(B) Analysis of liver mitochondrial acyl-CoA levels from mice that were under different fasting conditions. Wide-type mice were fasted for 0h, 6h, 12h, 24h or 48 hours, or the mice were fasted for 24 hours and then re-fed for 3 hours or 6 hours. Total hepatic tissues lysates were analyzed for succinyl-CoA and glutaryl-CoA levels by mass spectrometry metabolomic analysis. Error bars represent SEM.

Supplementary Figure S7C

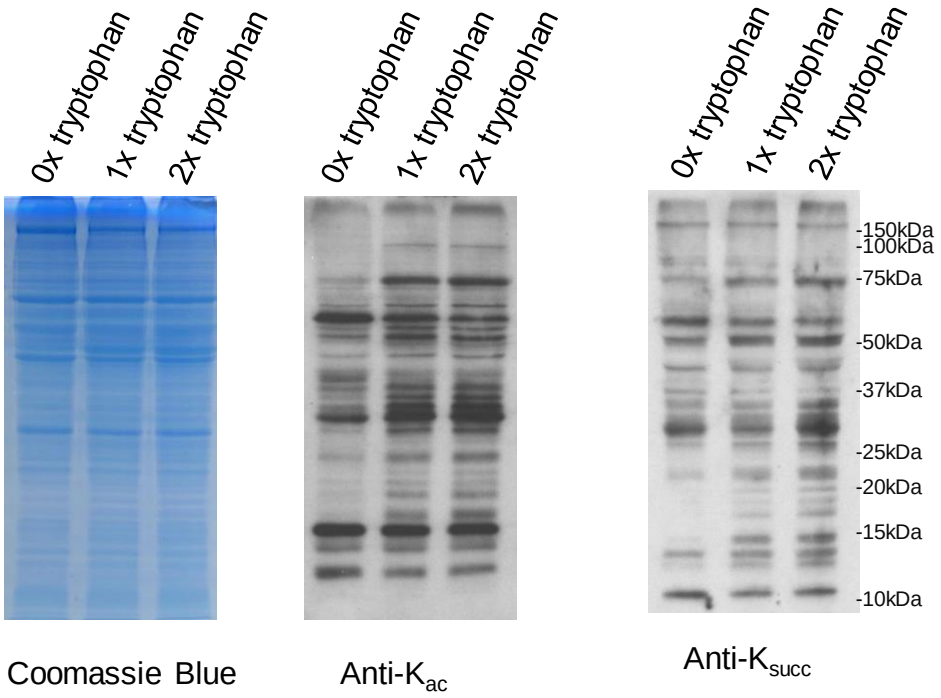

(C) *Drosophila* were fed with 0X, 1X or 2X tryptophan for 1 week and whole cell lysates were prepared for Western blotting analysis. Samples were analyzed for mitochondrial protein acetylation and succinylation.

Supplementary Figure S7D

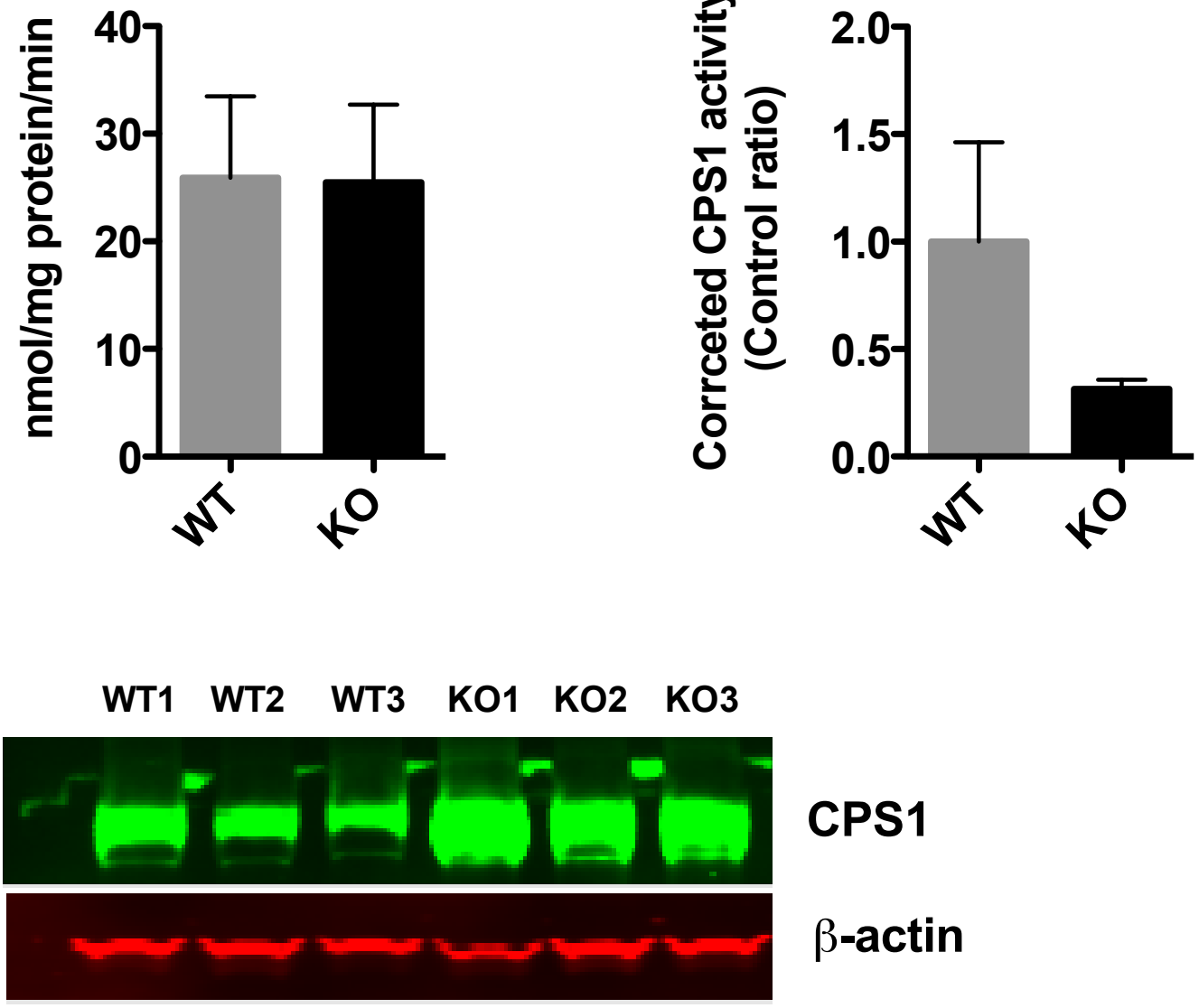

(D) CPS1 enzymatic activity was measured in hepatic lysates from wild-type and GCDHKO mice and normalized to total CPS1 protein levels. Error bars represent SEM.

Supplementary Figure S7E

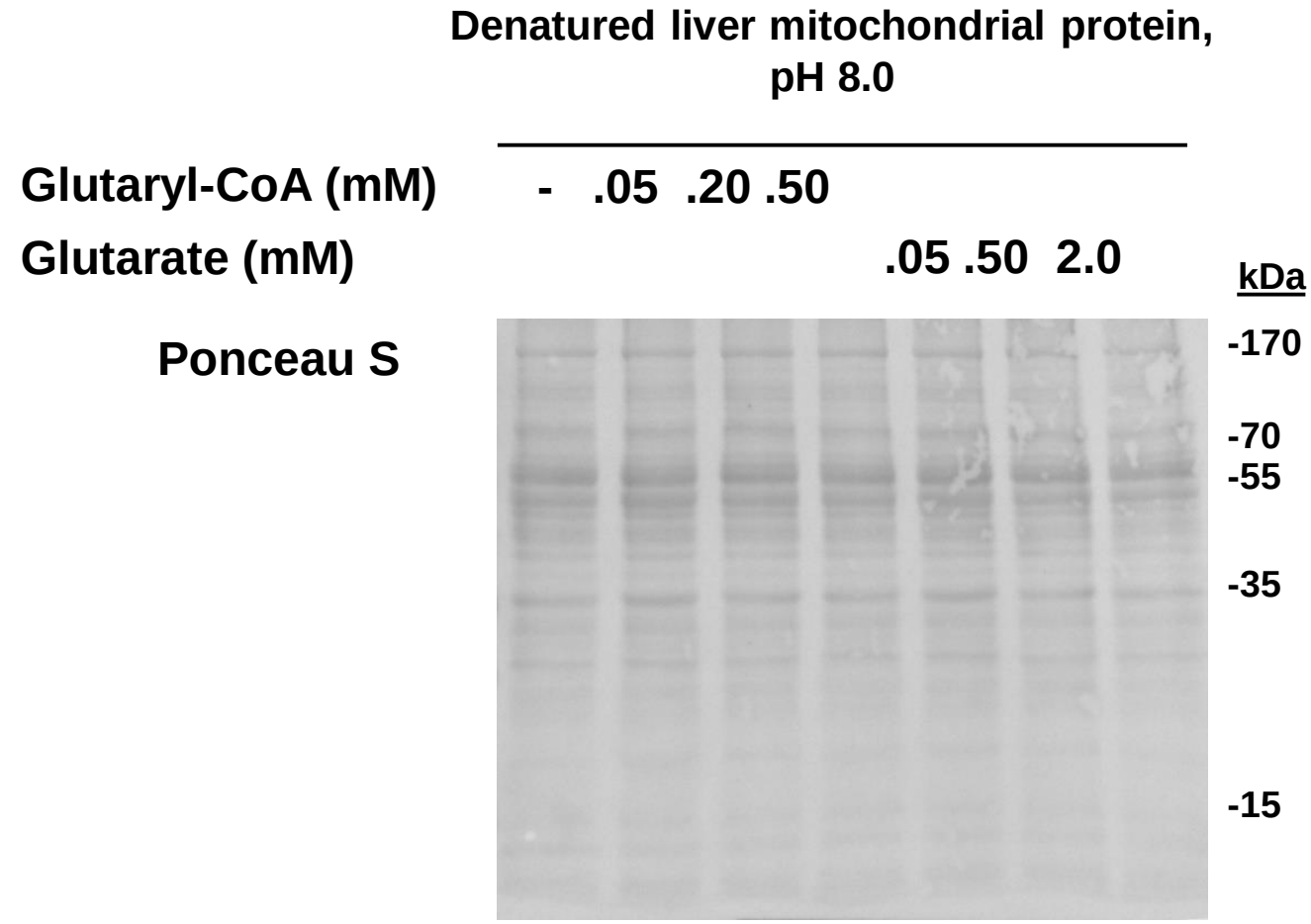

(E) Glutaryl-CoA or glutarate was incubated with heat-inactivated hepatic mitochondrial lysates and measured for total protein by Ponceau S staining.

Supplementary Figure S7F

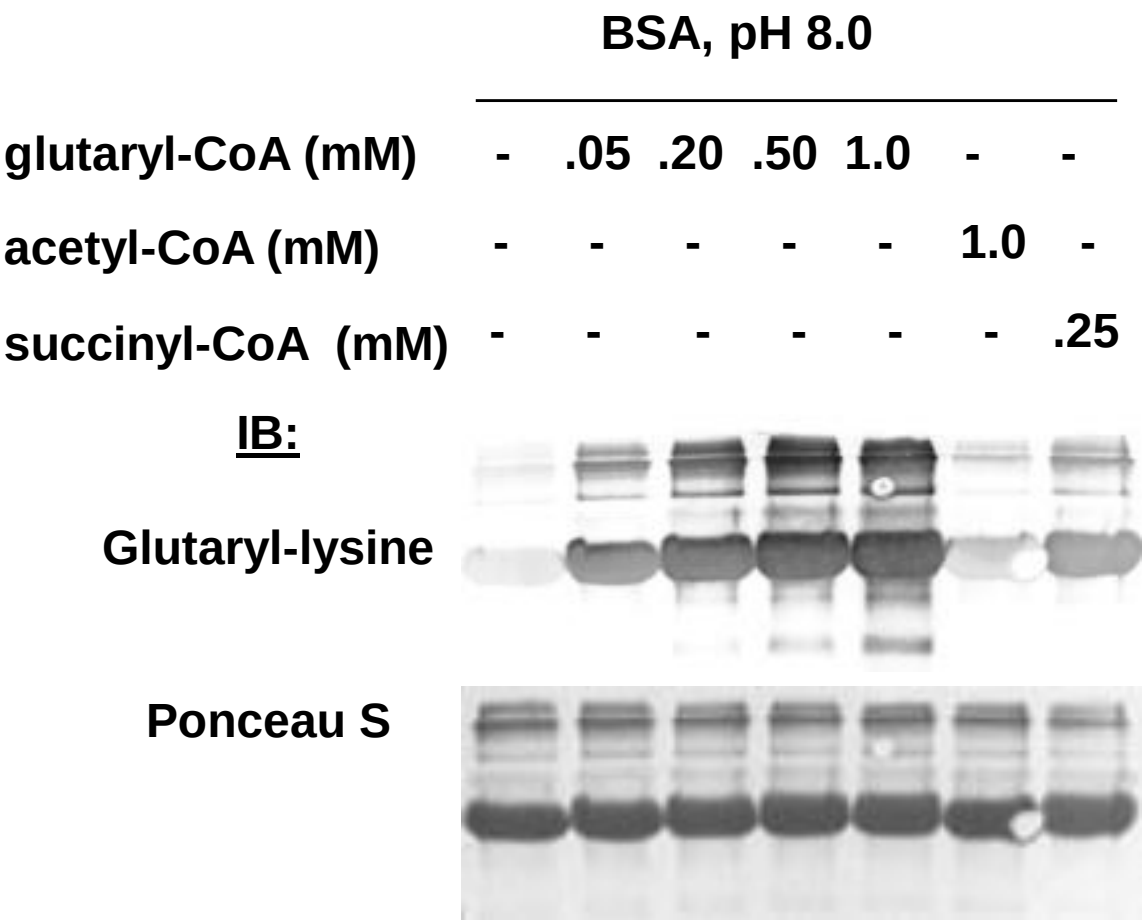

(F) Glutaryl-CoA, succinyl-CoA, or acetyl-CoA was incubated with BSA and measured for protein glutarylation using an anti-K_{glu} antibody, and normalized to total protein by Ponceau S staining.

Supplementary Experimental Procedures

Reagents. Ni-NTA agarose beads were purchased from QIAGEN; modified sequencing-grade trypsin from Promega; C18 ZipTips from Millipore Corporation; MS grade water and acetonitrile from Thermo Fisher; Trifluoroacetic acid (TFA) from Fluka; protein A beads from GE Healthcare; isotopic [2, 2, 4, 4-^{2}D] sodium glutarate from Cambridge Isotope Laboratories. The recombinant HDACs were purchased from BPS Bioscience. Additionally, expression plasmids for *SIRT5* wild-type and *SIRT5*-H158Y were constructed by Dr. Wei Gu (Columbia University). *SIRT5* expression vectors were expressed in *E. coli* and recombinant protein was purified. Other chemicals and reagents were obtained from the following suppliers: anti-K_{ac}, anti-K_{mal}, anti-K_{succ}, and anti-K_{glu} antibodies from PTM Biolabs, Inc; anti-prohibitin antibody from Abcam; anti-SIRT5 antibody from Thermo Fisher (PA5-13224). Chemical reagents not indicated were purchased from Sigma-Aldrich (highest available purity grade).

Chemical and peptide synthesis. Modified peptides were synthesized through commercial customer synthesis using Fmoc-protected amino acid residues. Fmoc-Lys (glutaryl)-OH, Fmoc-Lys (mono-tert-butyl glutaryl)-OH and fluorescent compounds for lysine deglutarylation and lysine deacetylation assays were synthesized as previously described (Peng et al., 2011).

Isotopic labeling using [2, 2, 4, 4-^{2}D] glutarate. HeLa cells were cultured at 37°C in a 95%/5% air/CO_2 incubator. The medium was then replaced with fresh DMEM medium

supplemented with 20 mM isotopic sodium [2, 2, 4, 4-^{2}D] glutarate. After 24 hours of treatment, the cells were washed with pre-cold PBS twice and then lysed with SDS sample buffer (25 mM Tris-Cl, pH 6.8, 1% SDS, 5% β-mercaptoethanol, 10% Glycerol).

Western blotting analysis, ECL. 20~40 μg of protein was resolved by SDS-PAGE, and transferred to polyvinylidene difluoride (PVDF) membrane. The membrane was blocked in TBSB (1x TBS buffer containing 0.05% Tween 20 and 3% BSA) at room temperature for 1hr and probed with appropriate primary antibodies. Following incubation with secondary antibodies, signals were detected by the ECL Western blot detection system. To carry out dot-blot assay, a gradient of peptide was spotted onto nitrocellulose (NC) membrane.

Western blotting, LI-COR. Whole-cell or crude mitochondrial protein extracts or CPS1 immunoprecipitates were resolved by SDS-PAGE and transferred to nitrocellulose membranes. The membranes were blocked in LI-COR buffer (0.6X PBS, 0.25% fish gelatin, 0.05% casein, and 0.02% azide) for 1h at room temperature and probed with primary antibody in LI-COR buffer/Tween (LI-COR buffer with 0.1% tween 20). After incubation with infrared dye-conjugated secondary antibodies the blots were developed using the LI-COR Odyssey Infrared Imaging System. Antibodies include: CPS1 (ab3682, Abcam), FLAG (Sigma-Aldrich), ATP synthase (Invitrogen), SIRT5 (ABE198, Millipore), acetyllysine (PTM Biolabs Inc.), succinyllysine and glutaryl-lysine (PTM Biolabs Inc., or generated in-house).

High-pH HPLC fractionation. High-pH HPLC fractionation was performed as previously described (Wang et al., 2011). Separation of peptides in HPLC was performed with a Luna C18, 250x10mm semi-preparative column containing 5 µM particles and together with a guard column (Phenomenex, Torrance, CA) at a flow rate of 4 mL/min. The organic solvent of the peptide fractions were removed in a Speed-Vac and then lyophilized.

In-solution tryptic digestion. Cells or tissues were lysed using SDS sample buffer and precipitated by 9 volumes of pre cold TCA/acetone (1:8) solution. The proteins were then tryptically digested following the procedure we described previously (Peng et al., 2011). Briefly, the protein precipitate was resuspended in 100 mM NH_4HCO_3 (pH 8.0) by sonication and digested at 37 °C for 16 hr by trypsin at an enzyme-to-substrate ratio of 1:50 (w/w). The sample was treated with 5 mM dithothreitol (DTT) to reduce disulfide bonds, and then 15 mM iodoacetamide was used to alkylate the resulting thiol group. The mixture was digested again at 37 °C for another 3 hr by adding additional trypsin (1:100 w/w). The resultant solution was then ready for the fractionation or immunoprecipitation with antibodies.

HPLC-MS/MS analysis. Tryptic digests or the enriched K_{glu} peptides was desalted with C18 ZipTips and loaded onto an in-house packed Jupiter C12 column (360 µm OD X 75 µm ID) connected to an Eksigent NanoLC-1D plus HPLC system (Eksigent Technologies). HPLC buffer A (0.1% formic acid in water, v/v) and HPLC buffer B (0.1% formic acid in acetonitrile, v/v) were used for HPLC analysis. Peptide samples were

separated with a 2-hr HPLC-gradient from 5% to 90% HPLC buffer B at a flow rate of 200 nL/min. The eluted peptides were ionized by a nanospray ion source and analyzed by an LTQ Velos Orbitrap mass spectrometer. High-resolution full MS spectra (from *m/z* 350–2000) were acquired using FTMS in the Orbitrap with resolution *R* = 60,000 at *m/z* 400. Lockmass ion from ambient air (m/z 445.120024) was used for internal calibration of all FT measurements. The twenty most intense ions from full MS analysis were sequentially isolated and fragmented by collision-activated dissociation (CAD) with a normalized energy of 35% in the linear ion trap. The dynamic exclusion duration for the data-dependent scan was 36 sec with a repeat count of 2. Singly charged ions are excluded for MS/MS fragmentation. 1E6 of AGC in the Orbitrap analyzer was used for full-scan analysis, 1E4 of AGC in the linear ion trap was used for MS/MS analysis. Signal threshold for CID acquisition was set at 5000.

Mass spectrometry data analysis. MS/MS data were analyzed by Mascot software (version 2.1) (Perkins et al., 1999) and MaxQuant software (version 1.0.13.13)(Cox and Mann, 2008). All the data were searched against either NCBI RefSeq *E.coli* k12 protein database (4123 sequences), IPI human protein database (v 3.70, 87069 sequences), or IPI mouse protein database (v 3.74, 56860 sequences). Cleavage enzyme was specified as trypsin, and the maximum number of missing cleavages was set to 3. Cysteine alkylation by iodoacetamide was specified as fixed modification, and methionine oxidation and lysine glutarylation (lysine +114.03169 Da) were specified as variable modifications.

Additional criteria used by standalone Mascot sequence alignment analysis were

as follows: Mass tolerances for precursor ions were set at 0.01 Da and for MS/MS were set at ±0.5 Da. Peak lists were generated by extract_msn.exe software (v5.0, Thermo Scientific).

Additional criteria used by MaxQuant software analysis for lysine glutarylome in mouse liver were as follows: peak generation and precursor mass recalibration were generated by MaxQuant software. Then Mascot search was performed by searching tandem mass spectra against IPI mouse database concatenated with reversed decoy database and common protein contaminants. The results of Mascot search were further processed by MaxQuant software. False discovery rate (FDR) thresholds for protein, peptide and modification site identification were all specified at 1%. Minimum peptide length was set at 6. Peptides with Mascot ion score lower than 20 as well as peptide C-terminal glutarylation were further removed. Identified K_{glu} peptides were selectively verified by manual inspection to ensure the highest possible stringency of mass spectrometry data analysis.

Co-elution analysis of K_{glu} peptides by HPLC-MS/MS. The *in vivo* K_{glu} peptide candidates from *E. coli* and HeLa cells, the synthetic counterparts, and their mixtures were analyzed by HPLC-MS/MS, respectively. Before each sample injection, extensive washing was carried out to avoid sample carryover in the HPLC system. Full MS and targeted CID MS/MS scans were acquired in the Orbitrap analyzer with a resolution of 30,000 and 7,500 at *m/z* 400, respectively. Amounts of synthetic peptides were adjusted to the similar levels of the corresponding *in vivo* peptides based on their precursor ion intensities.

***In vitro* deglutarylation assays.** Reactions were performed in a final volume of 50 µL per well in a 96-well microplate for fluorometric assays and in a final volume of 10 µL for peptides assays as previously described (Peng et al., 2011). Briefly, Boc-Lys(glu)-AMC (10 mM) or glutarylated peptides stocking solution and HDACs (HDAC1-11 or SIRT1-7 with 1 mM NAD^+) was added to 1x Reaction buffer (25 mM Tris-Cl, 130 mM NaCl, 3.0 mM KCl, 1 mM $MgCl_2$,1mM DTT, 0.1% PEG8000, pH 8.0) in sequence. The fluorometric reactions were stopped by adding 25 µL of developer solution (25 mM Tris-Cl, 130 mM NaCl, 3.0 mM KCl, 1 mM $MgCl_2$, 30% isopropanol, 0.01 mg/mL trypsin, pH 8.0) and analyzed on a fluorescence plate reader (The Wallac 1420 Workstation, IET Ltd, Vernon Hills, IL) with excitation set at 355 nm and emission measure at 460 nm after appropriate time of incubation. The peptide reactions were stopped by adding 10 µL of 100 mM HCl and 160 mM acetic acid and then analyzed by HPLC with a reverse phase C18 column (150x 4.6mm, 90A, 3.5um, Zorbax-SB, Invitrogen, Grand Island, NY) with a linear gradient of 22% to 38% for 15min (1mL/min). Product quantification was based on the area of absorption monitored at 280 nm, assuming hydrolysis of the acyl group does not affect the absorption. The k_{cat} and K_M values were obtained by curve-fitting the $1/V_{initial}$ versus 1/[S].

Principle of fluorescent assay for AMC-based substrates

In this assay, Boc-Lys (glu)-AMC with low fluorescence was synthesized as the HDAC-mimetic substrate and incubated with each of the 18 previously annotated HDACs. Any HDAC(s) with lysine deglutarylase activity would remove the glutaryl group from the

modified lysine residue, creating a proteolytic digestion site for trypsin (Figure S3A). After a subsequent tryptic digestion, the fluorescent molecule AMC will be released from the C-terminus of the lysine residue and generate an intense fluorescence signal.

Lipofectamine transfection. HEK293T cells stably expressing human SIRT5 shRNA or scramble RNA were transfected with human CPS1-FLAG plasmid DNA using Lipofectamine 2000 (Invitrogen) according to the manufacturer's recommendations. Cells were harvested 24 hr later. The human CPS1-FLAG construct was made by introducing a FLAG tag at the C-terminus of the full-length human CPS1 cDNA (Open Biosystems clone 9056755) and cloned into pSG5 expression plasmid (Invitrogen).

Calcium phosphate transfection. 50% confluent 293HEKT cells were transfected with human CPS1-FLAG plasmid using 20 µg human CPS1-FLAG DNA, 1x HBS, and 1 mM $CaCl_2$. Twenty four hours after transfection, transfection reagents were replaced with fresh media. Cells were harvested 24 hours later.

CPS1 immunoprecipitation from mouse liver. A fresh or thawed liver piece was minced in NP-40 lysis buffer and homogenized with 5 strokes in a Dounce homogenizer followed by further homogenization in chilled racks with a TissueLyser bead mill (Invitrogen) for 2 min at 30 Hz. After lysate centrifugation at 14,000 x *g* for 20 min to pellet, insoluble material the supernatant protein concentration was determined by the BCA protein assay (Sigma-Aldrich). Seven hundred fifty µg protein in 1 ml NP-40 lysis buffer was incubated end-over-end with 10 µL Protein A/G beads (Santa Cruz

Biotechnologies, sc-2003) for 1 h at 4 °C to preclear the lysate. The beads were pelleted and the supernatant added to fresh beads and 4 µL anti-CPS1 antibody (Abcam, #ab3682). After an overnight rotating incubation, the beads were pelleted, washed 3X with NP-40 lysis buffer and heated at 95 °C in SDS-PAGE sample loading buffer.

^{32}P-NAD^{+} consumption assay. Based on the method described by Du et al (Science, 2011), reactions were performed in a total volume of 10 µl in 50 mM Tris-HCl, pH 9.0, 4 mM $MgCl_2$, 50 mM NaCl, 0.5 mM DTT, and 0.5 µCi ^{32}P-NAD^{+} (PerkinElmer, NEG023X, 800 Ci/mmol) in the presence of either 2 µg acylated-BSA or 1 µg acylated-H4 peptide substrate. The reactions were incubated with 2 µg SIRT3-5 for 1 h at 37°C. At the end of the incubation, 2 µl of each reaction was spotted onto silica gel thin layer chromatography plates (Whatman Partisil LK6D) and resolved with ethanol:1M ammonium bicarbonate at 7:3. The plates were air-dried and exposed to a Kodak storage phosphorImaging screen SD230 (GE Healthcare) and the signal detected using a STORM820 phosphorimager (GE Healthcare). The sirtuin proteins used in the assay were bacterially expressed recombinant human SIRT5-(39-310)-6XHis and human SIRT3-(102-399)-6XHis (Hirschey et al., 2010). The bacterially expressed recombinant SIRT4 was mouse SIRT4-(24-333)-GST fusion protein obtained by cloning SIRT4 cDNA into pGEX-3X expression plasmid.

Chemical acylation of BSA and CPS1. Bovine serum albumin (BSA), (Sigma, fatty acid free, fraction V) at 2 mg/ml in 0.1 M sodium bicarbonate, pH 8, was mixed with

acetic, succinic, or glutaric anhydride (Sigma-Aldrich) at 5-fold molar excess over BSA lysine residues, to form acetyl-, succinyl-, and glutaryl-BSA, respectively. The reaction was incubated at room temperature for 30 min with continuous mixing, passed over a Sephadex G-25 column, and frozen at -20 °C. BSA lysine modifications were verified by mass spectrometry analysis by the Duke Proteomics Core Facility. Recombinant CPS1-FLAG protein overexpressed in and immunoprecipitated from HEK293T cells was acylated in an analogous reaction scaled-down to accommodate µg quantities of CPS1 protein. Following the reaction, 20 mM Tris-Cl, pH 8.0, was added to neutralize unreacted anhydride.

Acylation of histone H4 peptide. Histone H4 peptide amino acid residues 1-21 (Sigma-Aldrich) was acylated with the catalytic HAT domain of CBP in a 30uL reaction containing 50 mM Tris-HCl, pH 8, 50mM NaCl, 1 mM DTT, 10% glycerol, 10µg H4 peptide, 2 µg CBP, and 1 mM of either glutary-, acetyl-, or succinyl-CoA (Sigma-Aldrich). Following a 45 min incubation at 32 °C, CBP was removed by filtration using Microcon YM-50 centrifugation filters and the remaining modified H4 peptide lyophilized. Acylation of H4 peptide was confirmed by MS analysis at the Duke Proteomics Core Facility. The CBP catalytic HAT domain protein was obtained by overexpression and purification from *E. coli* as a GST fusion protein using the CBP-HAT-GST plasmid from Addgene (plasmid 21093).

Ammonia measurements. Ammonia present in cell culture media was quantified using the SYNCHON System from Beckman Coulter, Inc.

Ornithine measurements. Amino acids were analyzed using stable isotope dilution technique. The measurements were made by flow injection tandem mass spectrometry using sample preparation methods described previously (An et al., 2004). The data were acquired on Waters Acquity^{TM} UPLC system equipped with a TQ (triple quadrupole) detector and a data system controlled by MassLynx 4.1 operating system (Waters, Milford, MA).

CPS1 activity assay. CPS1 activity was assessed by measuring converted citrulline by a colorimetric method with modification (Chan et al., 2009; Pierson, 1980). 50-100 ug of liver protein was added to a 500 µL reaction mixture containing: 20 mM HEPES, 75 mM ammonium bicarbonate, 20 mM ATP, 40 mM magnesium chloride, 5 mM N-acetyl-glutamate, 5 mM L-ornithine, 3U ornithine transcarbamylase from E. coli. The reaction was allowed to proceed at 37 °C for 25 minutes. Chromogenic reagent A consisted of 850 mg of antipyrin in 100 mL of 40% sulfuric acid. Chromogenic reagent B consisted of 625 mg of 2,3 butadione monoxime in 5% acetic acid. For the stop solution and developer, equal parts of chromogenic reagent A and B were mixed and the reaction was terminated with 500 µL. The reaction was then developed for 15 minutes at 95 °C and read at 466 nm and referenced against a citrulline standard curve.

Protein complex enrichment analysis. Manually-curated CORUM core complexes data (Ruepp et al., 2008) were downloaded from http://mips.helmholtz-muenchen.de/genre/proj/corum/allComplexesCore.csv. Mouse and human complexes

indexed in the database were used for enrichment analysis using Fisher's exact test corrected by Benjamini-Hochberg method. The IPI were converted to Entrez gene ID for enrichment analysis. Mouse and human complexes were tested separately. Complexes with adjusted $p<0.01$ were considered significant.

Protein interaction network analysis. STRING 9.0 database (http://string-db.org/newstring_download/protein.links.v9.0.txt.gz) was used for protein interaction network enrichment analysis (Jensen et al., 2009). The IPI identifiers in this study were converted into the Ensemble protein ID using Ensemble BioMart version 0.7. High confidence interactions (>0.7) for mouse in the STRING database were extracted for protein-protein interaction analysis when at least one interacting protein is Lys glutarylated. MCODE plug-in toolkit (Bader and Hogue, 2003) visualized by Cytoscape (version 2.6.3) (Shannon et al., 2003) was used for network analysis.

Computational-based molecular modeling. All molecular modeling studies were conducted using Accelrys Discovery Studio 3.5 (Accelrys Software, Inc., San Diego, CA) and AutoDock 4.2 (The Scripps Research Institute, La Jolla, CA). All crystal structure coordinates were downloaded from the protein data bank (www.pdb.org). Utilizing the crystal structure of human SIRT5 co-crystallized with a succinylated histone H3K9 peptide (PDB ID: 3RIY (Du et al., 2011)), the additional modifications were built onto the co-crystallized Lys residue and each of the five respective structures (acetyl, malonyl, succinyl, glutaryl, and adipyl) were subjected to energy minimization utilizing the conjugate gradient minimization protocol with a CHARMm forcefield and the

Generalized Born implicit solvent model with simple switching (Feig et al., 2004). All minimization calculations converged to an RMS gradient of < 0.001 kcal/mol. Interaction energies were then calculated between the entire respective modified histone peptides and the NAD^+-bound SIRT5 using the implicit distance-dependent dielectric model and represents the sum total of both Van der Waals and electrostatic interactions.

The homology model of human carbamoyl phosphate synthase 1 (CPS1) was constructed with the MODELLER protocol (Eswar et al., 2008) using the crystal structure of *E. coli* carbamoyl phosphate synthetase (PDB ID: 1BXR; 40% identity, 60% similarity compared to the human sequence (Thoden et al., 1999)) as a template. The loop containing residues Thr405-Ala417 of the human CPS1 sequence, which shares no homology with the *E. coli* template, was refined using the LOOPER algorithm (Spassov et al., 2008), and the resulting final structure was subjected to energy minimization as described above. Figures were generated using Lightwave 11.5 (NewTek, Inc., San Antonio, TX), Modo 701 (Luxology, LLC, San Mateo, CA), and Photoshop CS6 (Adobe Systems, Inc., Mountain View, CA).

AutoDock 4.2 (The Scripps Research Institute, La Jolla, CA) was used to predict the potential binding between modified lysine and SIRT5 (Morris et al., 2009; Sanner, 1999). The crystal structures of SIRT5 in complex with NAD^+ (PDB entries 3RIY) was used as the receptor. The ligand and solvent molecules were removed from the crystal structures to obtain the docking grid, and the active site was defined using AutoGrid. The grid size was set to 60×40×60 points with grid spacing of 0.375 Å. The grid box was centered on the ligand from the corresponding crystal structure complexes. The

Lamarckian genetic algorithm was used for docking with the following settings: a GA runs number of 50, a maximum number of 25,000,000 energy evaluations, an initial population of 150 randomly placed individuals, a maximum number of 27,000 generations, a mutation rate of 0.02, a crossover rate of 0.80, and an elitism value (number of top individuals that automatically survive) of 1. The structures of modified lysine were built and geometry optimized using the program ChemBioOffice (PerkinElmer, Waltham, MA). The ligand was fully optimized inside the binding site during the docking simulations. Finally, the conformation with the lowest predicted binding free energy of the most frequently occurring binding modes in the SIRT5 active pocket was selected.

***In silico* analysis of deacylation activities of SIRT5**

To better understand how SIRT5 can catalyze these deacylation reactions, we performed *in silico* molecular modeling of SIRT5 bound to various acylated peptide substrates by two different strategies. First, to initially assess the potential feasibility of an interaction between SIRT5 and a glutaryl modification, we leveraged the known crystal structure of human SIRT5 co-crystallized with a succinylated histone H3K9 peptide (PDB ID: 3RIY) (Du et al., 2011). The succinyl modification was replaced with acetyl, malonyl, glutaryl (Figures 4B and S4C), and adipoyl modifications and each of the five structures underwent rigorous energy minimization. The distal boundary of the SIRT5 acyl binding pocket includes Tyr102 and Arg105 and interactions between these two residues and the negatively-charged carboxylate of the acyl modification are critical to optimal de-malonylase and de-succinylase activities of SIRT5 (Du et al., 2011). All

five structures maintained identical hydrogen bond interactions between the histone peptide, SIRT5, and NAD^+ (Figure S4D). The acetyl modification, lacking the carboxylate moiety, does not directly interact with Tyr102 or Arg105 (Figure S4D), however the malonyl, succinyl, and glutaryl modifications can be accommodated within the acyl binding site of SIRT5 that allow interaction with Tyr102 and Arg105 (Figure S4D). In contrast, the predicted binding of the adipoyl modification resulted in an altered orientation of the interaction of the terminal carboxylate with Arg105 and appears to interrupt or prevent hydrogen-bonding interactions with Tyr102 (Figure S4D), suggesting a reduced ability of SIRT5 to deacylate this putative modification. Interestingly, the predicted energy of the interaction was essentially identical between the malonyl-, succinyl-, or glutaryl-modified histone peptides and SIRT5, but was substantially less favorable involving either the acetyl or adipoyl modifications (Figure 4C). Differences in interaction energy were almost entirely due to changes in predicted electrostatic interactions (Figure 4C).

To further investigate whether glutaryl-lysine is a preferred substrate for SIRT5, we carried out *in silico* simulation experiments using AutoDock software (v4.2), to compare the binding conformations of five acyl lysine residues, lysine acetylation (K_{ac}), butyrylation (K_{bu}), crotonylation (K_{cr}), succinylation (K_{succ}), malonylation (K_{mal}) and glutarylation (K_{glu}), to SIRT5 (Figure S4E). Compared to K_{ac}, K_{bu}, and K_{cr}, the ligands, K_{mal}, K_{succ}, and K_{glu}, have lower binding energies (Table S2C). K_{glu} is bound to the O3' atom of NAD^+ and the backbone O atom of Val221 as K_{ac} and K_{bu} did (Figure S4E). Importantly, the terminal carboxyl group of K_{glu} makes bifurcated hydrogen bonds with Arg105. The strong charge-charge interaction stabilizes the ligand in the active pocket.

Besides, the O atom of Tyr102 also forms a hydrogen bond with one of the carboxyl group O atom. Importantly, these interactions may induce the ligand to form the bicyclic intermediate with NAD^+. These results support our enzymatic activity data, and can explain how glutaryl groups can be preferably removed by SIRT5, in a similar manner as lysine succinylation and malonylation, but not acetylation or adipoylation.

Fly Stocks and lysate preparation. All experiments were done using Canton S flies (*Drosophila melanogaster*) from the same cohort. After eclosion, adult flies were transferred into normal food, SY10% (10% sugar and yeast w/v). Flies were kept on this food until they were 11 days of age. On day 11, equal numbers of female and male flies were transferred into fresh vials containing one of 5 different treatment foods (0X, 1X, 2X Tryp). After 4 days on treatment food, 25 females and 25 males (except for the high-sugar treatment that sampled 30 females + 30 males) were collected and snap frozen in dry ice at -80 °C for Western blotting analysis. Mitochondrial lysate were extracted from mixed groups of male and female flies after 7 days on treatment foods.

For tryptophan-modified diets, all components of the diet were identical except for the concentration of tryptophan (0X, 1X or 2X). Below are the specific concentrations of major nutrients that were used in the tryptophan-modified diet. The 1x tryptophan food should be considered as a control diet compared with low (0X) or high (2X) tryptophan food.

Nutrients	1X Concentration (mg/ml)
Sucrose	17.12
Cholesterol	0.30
Phenylalanine	13.08
Histidine	9.03

Isoleucine	1.11
Lysine	20.01
Leucine	2.01
Methionine	8.67
Arginine	20.06
Threonine	19.92
Valine	21.97
Tryptophan	3.37
Alanine	26.49
Cysteine	0.37
Aspartic acid	18.87
Glutamic acid	1.34
Glycine	21.90
Asparagine	16.70
Proline	18.21
Glutamine	16.43
Serine	28.09
Tyrosine	0.66

Mitochondria isolation from *Drosophila.* The preparation method for *Drosophila* mitochondria was modified and developed from existing protocols (Miwa et al., 2003). Briefly, ~300 flies were immobilized by chilling on ice, decanted into a chilled mortar previously rinsed with isolation media (250 mM sucrose, 5 mM Tris–HCl, 2 mM EGTA, 1% w/v bovine serum albumin (BSA), pH 7.4 at 4 °C). After grinding the whole body, the resulting liquid was passed through two layers of absorbent muslin (Robert Bailey & Son plc, Stockport, England) and immediately centrifuged at 150 x *g* for 3 min at 4°C. The supernatant was passed through one layer of muslin and re-centrifuged at 9,000 x *g* for 10 min. The supernatant was discarded and the pellet was saved at -80 °C for western.

Purification of wild type and inactive mutant hSIRT5 proteins. Wild type hSIRT5 and a catalytically-inactive mutant hSIRT5 (H158Y) were over-expressed in *E. coli* BL21

(DE3) and purified as previous described (Peng et al., 2011). Briefly, the cells were cultured at 37 °C and then induced by 0.1 mM isopropyl-β-D-galactopyranoside (IPTG) at room temperature for 12 hr. The cells were spun down and lysed with PBS buffer containing 1% Tween-20, 20 mM β-mercaptoethanol and protease inhibitors cocktail (0.2 mM PMSF, 0.5 mM EDTA, 0.7 μg/mL pepstatin, and 0.5 mg/mL leupeptin) for 30 min. The mixture should be clear after brief sonication. The lysate was centrifuged at 20,000 *g*, 4 °C for 20 min and the supernatant was applied for affinity purification using Ni-NTA beads according to the manufacturer's instructions.

Animal experiments. Animal studies were performed according to protocols approved by the University of Michigan or Duke University. Wild type and SIRT5-deficient male mice were maintained on a standard chow diet or starved until they were sacrificed for experiments. Tissues were collected and homogenized immediately on ice by using a glass homogenizer. The homogenization buffer contained 0.2 M mannitol, 50 mM sucrose, 10 mM KCl, 1 mM EDTA, 10 mM Tris-Cl, protease inhibitor cocktail and deacetylase inhibitors (10 mM butyrate, 10 mM nicotinamide). Mitochondria were extracted as described previously (Lombard et al., 2007). Western blot was performed to examine the levels of global lysine glutarylation, succinylation and acetylation in liver and kidney mitochondria.

Functional annotation of K_{glu} proteins. Gene Ontology (GO) (Ashburner et al., 2000), Kyoto Encyclopedia of Genes and Genomes (KEGG) pathway (Kanehisa and Goto, 2000) and Pfam domain (Finn et al., 2008) enrichment analysis were performed using DAVID (The Database for Annotation, Visualization and Integrated Discovery) tools with

the total mouse genome information as the background (Huang da et al., 2009). GO biological process, molecular function and cellular compartment categories were analyzed separately using GO Fat database of DAVID. The adjusted p-value (Benjamini) cutoff is <0.01.

Enrichment analyses of metabolic pathways using KEGG database

KEGG database enrichment analyses (Figure S5G and Table S4D) showed that lysine glutarylation occurs on many metabolic enzymes involved in valine, leucine, and isoleucine degradation (30/46, $p=5.6\times10^{-36}$, Figure S5H), butanoate (20/37, $p=5.9\times10^{-21}$) and propanoate (18/30, $p=5.7\times10^{-20}$) metabolism, fatty acid metabolism (21/45, $p=1.2\times10^{-20}$, Figure S5I), and the TCA cycle (13/31, $p=1.5\times10^{-11}$). In addition, this analysis also showed that lysine glutarylation was enriched in tryptophan metabolism ($p=3.5\times10^{-10}$, Figure S5J) and lysine degradation ($P=8.2\times10^{-9}$, Figure S5K), which are two metabolic pathways that directly generate glutaryl-CoA, implying a potential regulatory impact of protein glutarylation on metabolic pathways involving glutaryl-CoA in cells.

Domain enrichment analysis using Pfam database

Functional domains are the basic elements that determine the biological properties of a protein. To investigate possible protein domains associated with lysine glutarylation, we carried out domain enrichment analysis using the Pfam database. In this analysis, acyl-CoA dehydrogenase domains, the enoyl-CoA hydratase/isomerase family, and the aldehyde dehydrogenase family were most overrepresented among K_{glu} proteins

(Figure S5L and Table S4E). These data, together with GO and KEGG enrichment analyses, strongly suggest a potential role for lysine glutarylation in oxidative metabolism.

Protein complexes and interaction networks of lysine glutarylated proteins using CORUM and STRING databases.

To identify protein complexes enriched in lysine glutarylation substrates, we performed enrichment analysis with manually annotated CORUM core complexes database (Ruepp et al., 2010). Since experimentally validated mouse complexes are very limited, we considered both mouse and human complexes in the CORUM database by using both mouse genes and their corresponding human orthologs for enrichment analysis, based on the assumption that core protein complexes are evolutionarily conserved between mouse and human. This analysis showed that F1F0-ATP synthase (p=3.8×10^{-8}) and respiratory chain complex I (p=4.0×10^{-3}) were enriched (Figure S5M and Table S4F). Consistent with GO analysis results, these complexes localize to mitochondria, and are functionally related with metabolism and aerobic respiration. Finally, to study protein interaction networks of lysine glutarylation substrates, we used the STRING database and the MCODE algorithm to investigate the K_{glu} interactome (Figure S5N), and identified 31 highly inter-connected clusters (Table S4G and Figure S5O). Most of these protein networks are associated with metabolic pathways, and are localized to mitochondria, consistent with our other bioinformatic analyses.

Protein glutarylation. A 5 mM solution of glutaryl-CoA lithium salt (Sigma) and a 10 mM solution of glutaric acid (Sigma) were each made in 50 mM HEPES, 150 mM NaCl, and adjusted to pH 8.0 at 37 °C. Dilutions were made using 50 mM HEPES (pH 8.0 at 37°C), 150 mM NaCl as the diluent. Liver mitochondria frozen in 50 mM HEPES pH 8.0, 150 mM NaCl at 1.5 µg/µl were thawed on ice and sonicated twice for 15 seconds on ice. The sample was cleared by centrifugation at 10,000 x g for 5 min at 4 °C. Twenty microliters of soluble mitochondrial protein supernatant were denatured at 95 °C for 10 min followed by centrifugation to collect buffer condensation and to pellet the denatured protein. Denatured mitochondrial protein was cooled on ice and resuspended with pipetting prior to the addition of the appropriate dilution of glutaryl-CoA or glutaric acid to generate the indicated final concentrations of glutaryl-CoA or glutaric acid in a total sample volume of 40 µl. Samples were incubated for 6 hours at 37 °C at 400 rpm in an Eppendorf Thermomixer. Sample tubes were briefly centrifuged every 2 hours during the incubation to minimize condensation, followed by gentle resuspension with pipetting. Following the incubations, SDS sample buffer was added to the samples which were then separated with 12% SDS-PAGE followed by Western blotting with a home-made glutaryl-lysine antibody. For experiments with BSA, 2 µg/µl solutions of non-acetylated, fatty-acid free BSA were made in 50 mM HEPES, 150 mM NaCl and adjusted to pH 8.0 at 37 °C. Twenty microliters of each BSA solution was added to 20 µl of the appropriate dilution of glutaryl-CoA and incubated in an Eppendorf Thermomixer as previously described.

Supplementary References:

An, J., Muoio, D.M., Shiota, M., Fujimoto, Y., Cline, G.W., Shulman, G.I., Koves, T.R., Stevens, R., Millington, D., and Newgard, C.B. (2004). Hepatic expression of malonyl-CoA decarboxylase reverses muscle, liver and whole-animal insulin resistance. Nat Med *10*, 268-274.
Ashburner, M., Ball, C.A., Blake, J.A., Botstein, D., Butler, H., Cherry, J.M., Davis, A.P., Dolinski, K., Dwight, S.S., Eppig, J.T., et al. (2000). Gene ontology: tool for the unification of biology. The Gene Ontology Consortium. Nat Genet *25*, 25-29.
Bader, G.D., and Hogue, C.W. (2003). An automated method for finding molecular complexes in large protein interaction networks. BMC Bioinformatics *4*, 2.
Chan, C.H., Ramirez-Montealegre, D., and Pearce, D.A. (2009). Altered arginine metabolism in the central nervous system (CNS) of the Cln3-/- mouse model of juvenile Batten disease. Neuropathol Appl Neurobiol *35*, 189-207.
Cox, J., and Mann, M. (2008). MaxQuant enables high peptide identification rates, individualized p.p.b.-range mass accuracies and proteome-wide protein quantification. Nat Biotechnol *26*, 1367-1372.
Du, J., Zhou, Y., Su, X., Yu, J.J., Khan, S., Jiang, H., Kim, J., Woo, J., Kim, J.H., Choi, B.H., et al. (2011). Sirt5 is a NAD-dependent protein lysine demalonylase and desuccinylase. Science *334*, 806-809.
Eswar, N., Eramian, D., Webb, B., Shen, M.Y., and Sali, A. (2008). Protein structure modeling with MODELLER. Methods Mol Biol *426*, 145-159.
Feig, M., Onufriev, A., Lee, M.S., Im, W., Case, D.A., and Brooks, C.L., 3rd (2004). Performance comparison of generalized born and Poisson methods in the calculation of electrostatic solvation energies for protein structures. J Comput Chem *25*, 265-284.
Finn, R.D., Tate, J., Mistry, J., Coggill, P.C., Sammut, S.J., Hotz, H.R., Ceric, G., Forslund, K., Eddy, S.R., Sonnhammer, E.L., et al. (2008). The Pfam protein families database. Nucleic Acids Res *36*, D281-288.
Hirschey, M.D., Shimazu, T., Goetzman, E., Jing, E., Schwer, B., Lombard, D.B., Grueter, C.A., Harris, C., Biddinger, S., Ilkayeva, O.R., et al. (2010). SIRT3 regulates mitochondrial fatty-acid oxidation by reversible enzyme deacetylation. Nature *464*, 121-125.
Huang da, W., Sherman, B.T., and Lempicki, R.A. (2009). Bioinformatics enrichment tools: paths toward the comprehensive functional analysis of large gene lists. Nucleic Acids Res *37*, 1-13.
Jensen, L.J., Kuhn, M., Stark, M., Chaffron, S., Creevey, C., Muller, J., Doerks, T., Julien, P., Roth, A., Simonovic, M., et al. (2009). STRING 8--a global view on proteins and their functional interactions in 630 organisms. Nucleic Acids Res *37*, D412-416.
Kanehisa, M., and Goto, S. (2000). KEGG: kyoto encyclopedia of genes and genomes. Nucleic Acids Res *28*, 27-30.
Lombard, D.B., Alt, F.W., Cheng, H.L., Bunkenborg, J., Streeper, R.S., Mostoslavsky, R., Kim, J., Yancopoulos, G., Valenzuela, D., Murphy, A., et al. (2007). Mammalian Sir2 homolog SIRT3 regulates global mitochondrial lysine acetylation. Mol Cell Biol *27*, 8807-8814.
Miwa, S., St-Pierre, J., Partridge, L., and Brand, M.D. (2003). Superoxide and hydrogen peroxide production by Drosophila mitochondria. Free Radic Biol Med *35*, 938-948.

Morris, G.M., Huey, R., Lindstrom, W., Sanner, M.F., Belew, R.K., Goodsell, D.S., and Olson, A.J. (2009). AutoDock4 and AutoDockTools4: Automated docking with selective receptor flexibility. J Comput Chem *30*, 2785-2791.
Peng, C., Lu, Z., Xie, Z., Cheng, Z., Chen, Y., Tan, M., Luo, H., Zhang, Y., He, W., Yang, K., et al. (2011). The first identification of lysine malonylation substrates and its regulatory enzyme. Mol Cell Proteomics *10*, M111 012658.
Perkins, D.N., Pappin, D.J., Creasy, D.M., and Cottrell, J.S. (1999). Probability-based protein identification by searching sequence databases using mass spectrometry data. Electrophoresis *20*, 3551-3567.
Pierson, D.L. (1980). A rapid colorimetric assay for carbamyl phosphate synthetase I. J Biochem Biophys Methods *3*, 31-37.
Ruepp, A., Brauner, B., Dunger-Kaltenbach, I., Frishman, G., Montrone, C., Stransky, M., Waegele, B., Schmidt, T., Doudieu, O.N., Stumpflen, V., et al. (2008). CORUM: the comprehensive resource of mammalian protein complexes. Nucleic Acids Res *36*, D646-650.
Ruepp, A., Waegele, B., Lechner, M., Brauner, B., Dunger-Kaltenbach, I., Fobo, G., Frishman, G., Montrone, C., and Mewes, H.W. (2010). CORUM: the comprehensive resource of mammalian protein complexes--2009. Nucleic Acids Res *38*, D497-501.
Sanner, M.F. (1999). Python: a programming language for software integration and development. J Mol Graph Model *17*, 57-61.
Shannon, P., Markiel, A., Ozier, O., Baliga, N.S., Wang, J.T., Ramage, D., Amin, N., Schwikowski, B., and Ideker, T. (2003). Cytoscape: a software environment for integrated models of biomolecular interaction networks. Genome Res *13*, 2498-2504.
Spassov, V.Z., Flook, P.K., and Yan, L. (2008). LOOPER: a molecular mechanics-based algorithm for protein loop prediction. Protein Eng Des Sel *21*, 91-100.
Thoden, J.B., Wesenberg, G., Raushel, F.M., and Holden, H.M. (1999). Carbamoyl phosphate synthetase: closure of the B-domain as a result of nucleotide binding. Biochemistry *38*, 2347-2357.
Wang, Y., Yang, F., Gritsenko, M.A., Wang, Y., Clauss, T., Liu, T., Shen, Y., Monroe, M.E., Lopez-Ferrer, D., Reno, T., et al. (2011). Reversed-phase chromatography with multiple fraction concatenation strategy for proteome profiling of human MCF10A cells. Proteomics *11*, 2019-2026.